Advanced Imaging in Glioma Treatment

Verburg, N.

2020

document version
Publisher's PDF, also known as Version of record

Chapter 1

Introduction

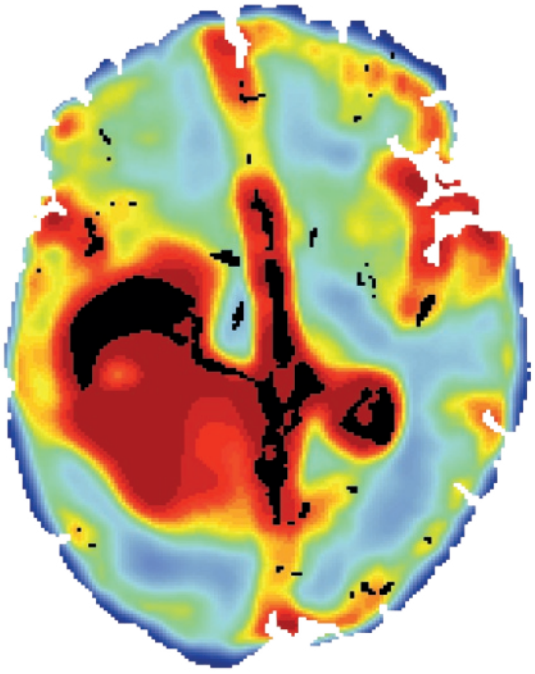

Despite multidisciplinary treatment, the prognosis for diffuse glioma patients remains poor with a two-year survival of 26% for the most malignant subtype (glioblastoma) and 70% to 85% for the least malignant subtypes (diffuse astrocytoma or oligodendroglioma).[1]

Diffuse glioma treatment consists of surgical resection, mostly followed by adjuvant chemo- and/or radiotherapy, depending on clinical condition, age and subtype.[2] Surgical resection aims to provide adequate tissue for histologic and molecular tumor characterization, to relieve mass effect, to achieve cytoreduction and to reduce symptoms. To achieve these goals, it is imperative to be able to reliably distinguish tumor tissue from normal brain tissue, which can be quite difficult since diffuse gliomas grow infiltratively into surrounding normal brain. Diffuse glioma infiltration can be visualized using several imaging modalities, besides fluorescence guidance and intraoperative probes, enabling tumor delineation. This visualization is used to guide not only the surgical resection, but also the postoperative radiotherapy planning.

The imaging modality currently used for diffuse glioma delineation is magnetic resonance imaging (MRI), especially the MRI sequences T1-weighted (T1w) after a gadolinium-based contrast agent (T1G), and T2- (T2w) or Fluid-Attenuated Inversion Recovery-weighted (FLAIR). It is clear, however, that the accuracy of these sequences for identification of diffuse glioma infiltration is suboptimal, as diffuse gliomas recur even after a so-called radiologically complete resection:[3,4] over 80% of recurrences are directly adjacent to the resection cavity and diffuse glioma cells have been detected outside abnormalities on all of these MRI sequences.[5-8] Identification of more accurate imaging modalities or MRI sequences could lead to improved delineation of diffuse glioma. Alternative advanced MRI sequences, like diffusion- and perfusion-weighted MRI, magnetic resonance spectroscopy imaging (MRSI) and other imaging modalities such as positron emission tomography (PET), are available and might be more accurate for the identification of diffuse glioma infiltration. More accurate delineation will help to guide resections beyond current MRI abnormalities, as well as to identify patients with diffuse glioma infiltration beyond meaningful surgical therapy, to guide radiotherapy, to evaluate treatment response and to detect tumor progression.

In order to answer the question: “Which MRI sequence, PET tracer, or combination of MRI sequence(s) and/or PET tracer(s) is the most accurate for the detection of diffuse glioma infiltration?”, the work in this thesis shows the current evidence for imaging accuracy, the use of quantitative PET, the direct comparison of multiple MRI sequences

and PET tracers and the quantification of diffuse glioma infiltration, using histology, molecular biology and imaging. To appreciate the ensuing chapters, this introduction first elaborates on diffuse glioma and several imaging techniques nowadays available for the detection of diffuse glioma infiltration.

GLIOMA

Epidemiology

Diffuse gliomas are the most common primary brain tumors in adults.[1] They account for the majority (96%) of all gliomas, are all WHO grade II-IV, and show extensive infiltrative growth into the surrounding CNS parenchyma.[9,10] In this thesis the term "glioma" will be used instead of "diffuse glioma' to increase readability. Based on histopathological assessment and molecular markers, gliomas are divided into subtypes.[9] Glioblastoma (WHO grade IV) is the most common, and most malignant, subtype and accounts for about 59% of all diffuse gliomas.[10]

The incidence of glioma varies between countries, with the highest rates in Europe and the lowest rates in Asia, and is higher in men than in women, with a ratio between 1.0 and 2.7. In the Netherlands the incidence (per 100,000 people, age ≥ 15, per year) of glioma in men is 7.5 and in women 5.0 (ratio 1.5). Racial variation exists, with higher incidences observed in the white population (8.3 in men and 6.0 in woman), compared to the black population (4.4 in men and 3.6 in women).[11] Age at primary diagnosis is higher for glioblastoma (median age 65 years) than for grade II gliomas (median age oligodendroglioma 43 and astrocytoma 48 years).[10]

The 10-years survival of glioma is 16-18%, placing it among the five cancer types with the worst survival rate. The potential years of life lost, i.e. the number of years not lived before a given reference age, is the highest of all cancer types, with an average of 16 life years lost. Glioma, together with pancreatic cancer, has the highest cancer-specific contribution to the all-cause potential years of life lost.[12]

Biology

The three major categories of glial cells are astrocytes, oligodendrocytes and ependymal cells.[13] These cells normally support and protect the neurons, maintain homeostasis and form myelin. Gliomas have been thought to arise from the precursors of glial cells: neural

stem cells and glial progenitor cells. Neural stem cells are self-renewing, can differentiate into both neural and glial cell types, and are found in specific parts of the brain, whereas glial progenitor cells are also self-renewing, but can only divide into glial cell types and are found throughout the brain.[14]

The transformation of these precursors into a diffuse glioma is thought to be the result of an accumulation of molecular events, which determine the glioma subtype. In about 50% of gliomas, the first event is mutation in the isocitrate dehydrogenase 1 (*IDH1*) gene, hence they are named IDH-mutant gliomas.[15] The mutated *IDH1* gene drives oncogenesis by influencing the methylation of genes,[16] a process that prevents the gene to be transscripted by adding a methyl-group to a nucleotide at the start site (promoter) of the gene.[17] By adding methyl-groups to onco-repair genes and removing them from oncogenes, cancer cells receive a growth advantage.[16] The second event in 37% of these IDH-mutant tumors is the complete loss of chromosome arms 1p and 19q (1p/19q co-deletion), resulting in the oligodendroglioma subtype (WHO grade II or III). The remaining 63% without 1p/19q co-deletion become astrocytoma subtype (WHO grade II or III). The diffuse gliomas without *IDH1* gene mutations, so-called IDH-wildtype, are now considered as belonging to the diffuse astrocytoma group. About 80% of these tumors are histologically WHO grade IV (glioblastoma), and many of the remaining tumors that would histologically be designated WHO grade II or III have molecular features indicating WHO grade IV behavior as well.[15,18,19] A schematic overview of this classification is presented in Figure 1. Other molecular events have been studied and are known to contribute to glioma oncogenesis, however, they fall outside the scope of this introduction.[20]

Progression into higher WHO grades is a hallmark of glioma. This malignant progression is based on histopathological features such as mitotic activity, microvascular proliferation and necrosis. At a molecular level, there is a difference between malignant progression of IDH-mutant and IDH-wildtype glioma. Progression of IDH-mutant glioma is driven by specific oncogenic pathways, resulting in a clear genetic and epigenetic difference between lower and higher grade IDH-mutant glioma.[22] In IDH-wildtype glioma, as described above, genetic differences between histologically lower and higher grade glioma are minimal.[23]

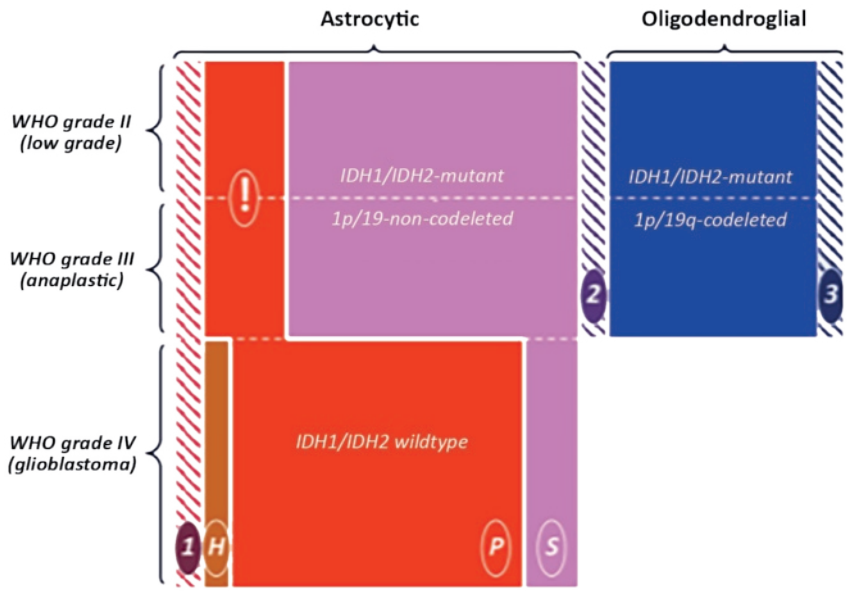

Figure 1 | World Health Organization 2016 Classification of diffuse gliomas. The hatched bars with the numbers 1,2 and 3 represent tumors where adequate molecular testing cannot be performed or the test results are inconclusive. The exclamation mark represents a group of histologically lower grade astrocytic tumors that show molecular characteristics and behave like glioblastoma. The orange bar with the letter "H" represents diffuse gliomas with a histone H3 K27M mutation, a characteristic of diffuse midline gliomas that occur especially in children. The letter "P" and "S" stand for primary and secondary, indicating if a tumor started as glioblastoma (P) or originated as lower grade (S).[21]

Blood-brain barrier (BBB) disturbance is another hallmark of glioma, occurring in most high- and some low-grade gliomas. The BBB is formed by, among others, endothelial tight junctions induced by astrocytic endfeet that cover the entire cerebral vasculature. These astrocytic endfeet are displaced by glioma cells, thereby causing a focal disruption of the BBB.[24] This disruption leads to vasogenic edema, which in its turn can lead to increased cranial pressure.[25]

Glioma infiltration

Diffuse glioma are named 'diffuse' due to widespread infiltration of glioma cells in the surrounding brain. This infiltration starts early in the oncogenesis by proliferating tumor cells detaching from the tumor mass and becoming peritumoral migrating

cells.[26] Migration depends on, among others, cerebrospinal fluid, as well as anatomical structures such as white matter tracts and blood vessels. Migrating glioma cells have been reported far away from the tumor core, even into the contralateral hemisphere.[4,27]

The degree, defined as the percentage of tumor cells among non-tumor cells, and extent, defined as distance from the tumor core, of glioma infiltration in the surrounding brain are difficult to quantify. The degree of infiltration would ideally be quantified by determining for each single cell if it is tumor or normal brain. Single cell transcriptional analysis is promising for this purpose, however, very limited in the volume of tissue it can process.[27] Histopathological assessment of the degree of glioma infiltration has long been the standard, with cellularity and Ki67-index as foremost metrics. Cellularity can be assessed by counting the number of cells per mm^2 on a histological slide. The Ki67-index is the fraction of cells with the protein Ki-67 present in their nuclei, which occurs during all active phases of the cell cycle. Therefore, Ki-67 can also occur in non-tumor cells. Presence of Ki-67 is determined on histological slides after MIB-1 antibody immunohistochemical staining. Both cellularity and Ki-67 index, however, are non-specific markers, meaning that they can also be higher than normal without glioma infiltration. Also, migrating glioma cells demonstrate lower proliferation rates and therefore a lower Ki-67 index.[26] An alternative is immunohistochemistry for IDH1 R132H mutant protein, which allows identification of single glioma cells, yet only for gliomas with a IDH1 R132H mutation. The 2007 WHO guideline for central nervous system tumors concluded that all approaches for the identification of glioma infiltration have been limited by the fact that single neoplastic glial tumor cells frequently cannot be distinguished from normal or reactive cells on grounds of morphology or immunocytochemical profile.[28]

As with the degree, identification of the extent of glioma infiltration is problematic. Most evidence comes from post-mortem studies, demonstrating a variation in the extent of infiltration between gliomas. Limited invasion, defined as infiltrating cells less than 1 cm from the edge of the gross tumor, was reported in 20–27%, extensive spread, defined as infiltration more than 3cm from the gross tumor, in 20% and dissemination in 8% of glioblastomas.[29] The term “whole brain disease” or “systemic brain disease” has been used to describe glioma,[30] however, this is not applicable to all gliomas. Also, post-mortem studies reflect the end-stage of the disease and do not represent the daily practice of newly-diagnosed glioma.

Clinical presentation

Symptoms at initial presentation vary according to growth speed and location. Growth speed depends on the subtype of glioma, with the highest in glioblastoma and the lowest in low-grade glioma.[31,32] Fast-growing high-grade tumors typically result in signs of raised intracranial pressure, such as progressive headaches worse at night, morning nausea and vomiting, drowsiness, blurred vision from papilledema, and horizontal diplopia from cranial nerve VI palsy. Focal symptoms, due to mass effect or tumor infiltration, often develop early in the disease and depend on the location. Major categories of symptoms are disturbances of language, weakness, numbness, visual field defects and cognitive dysfunction. Epileptic seizures occur in 30–50% of patients with a glioblastoma. Slower-growing low-grade gliomas typically present with epileptic seizures, occurring in 75% of those patients,[33] and focal symptoms develop later in the disease. The overall clinical condition of a patient is assessed with the Karnofsky Performance Scale (KPS), ranging from 0 to 100, with a higher score reflecting a better condition.[34] This KPS is an important prognostic and predictive marker in glioma treatment.[35] Finally, 4–10% percent of patients with a low-grade glioma is asymptomatic and the tumor is incidentally found on imaging.[36,37]

Radiological diagnosis

Imaging is indispensable in the diagnosis, treatment and follow-up of glioma, with MRI as standard modality. Different MRI sequences can visualize gliomas. The suggested minimal MRI sequences for the radiological diagnosis of a glioma are T1w, T2w, FLAIR and T1G MRI.[38] A major radiological feature for glioma classification is the presence or absence of contrast enhancement on T1G MRI. Gliomas with contrast enhancement are called ‘enhancing’ and gliomas without contrast enhancement ‘non-enhancing’. Non-enhancing gliomas are low-grade in 75%, with an increased risk of higher grade for older patients. Enhancing gliomas are high-grade in 87%.[39] Other imaging characteristics also differ between subtypes as presented in Table1. Exemplary images of the different subtypes are displayed in Figure 2.

Histopathological diagnosis

Gliomas are diagnosed using pathological assessment of biopsied or resected tumor tissue. Historically, this diagnosis was purely histopathological, however, recent advances in molecular biology have led to a combined histopathological and molecular classification.[9,21]

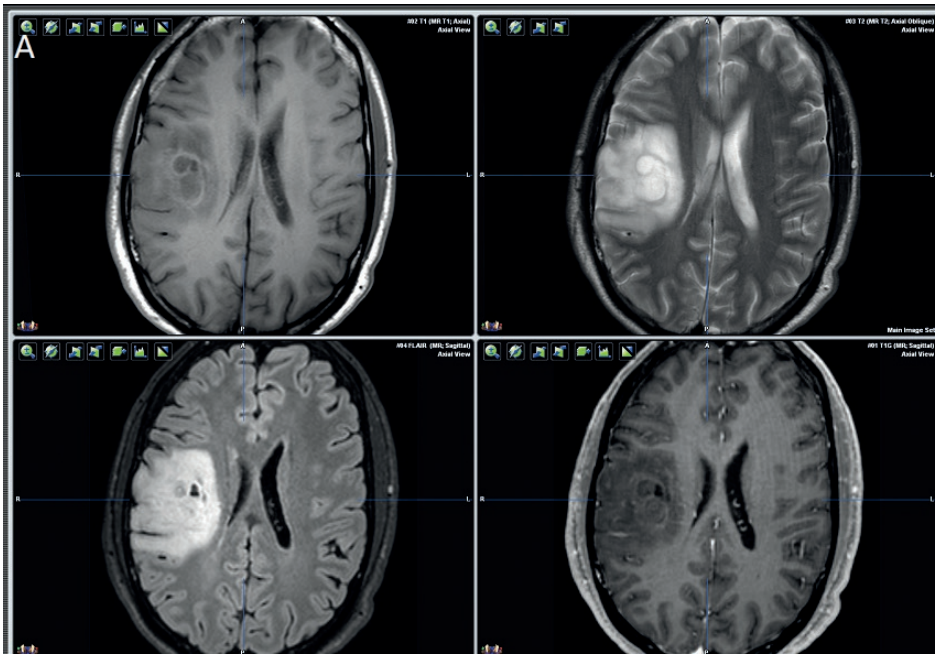
A

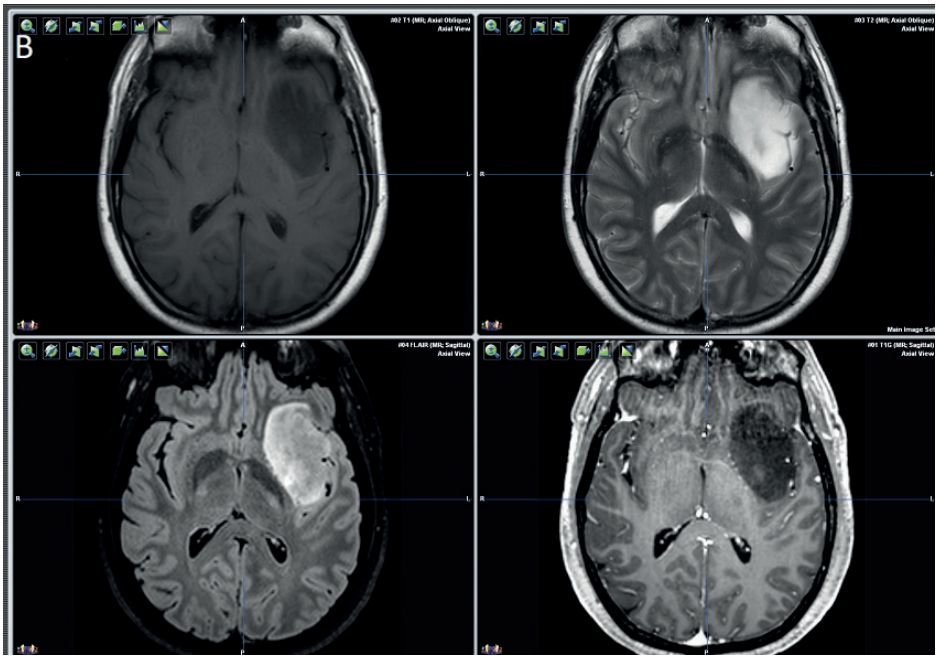
B

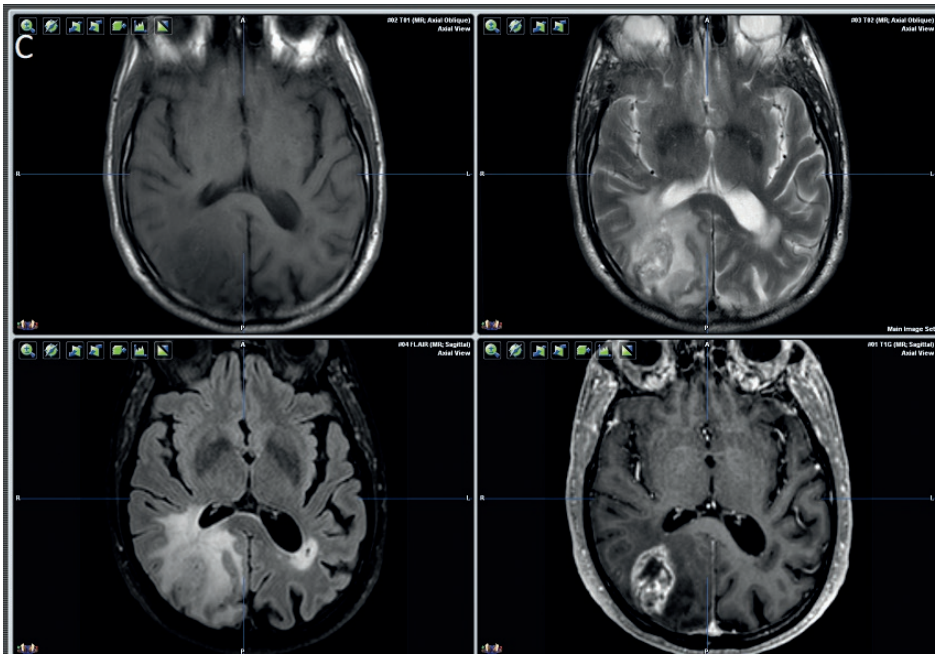

Figure 2 | Examples of standard MRI for different glioma subtypes

Axial T1w (top row left), T2w (top row right), FLAIR (bottom row left) and T1G (bottom row right) MRI images. Of A) patient with a right frontoparietal oligodendroglioma, IDH-mutant and 1p/19q-codeleted, B) patient with a left temporal diffuse astrocytoma, IDH-mutant, and C) patient with a right parieto-occipital glioblastoma, IDH-wildtype.

Histologically, oligodendroglioma consist of tumors cells with a prominent oligodendrocytic phenotype, including a round nucleus with a clear halo of cytoplasm resulting in a 'fried egg' appearance (Figure 3A). In contrast, astrocytoma generally show tumor cells with variable eosinophilic cytoplasms and/or eosinophilic cell processes and more elongated nuclei with variable nuclear atypia (Figure3B).[40] Oligoastrocytoma harbor tumor cells with both features, however, molecular insights have almost rendered this diagnosis obsolete. Besides the type of tumor cell, histological characteristics of malignancy are used to classify a glioma as WHO grade II, III or, in case of astrocytic gliomas, IV.

Table 1 | Typical imaging characteristics of standard MRI sequences and CT for the different glioma subtypes.[41,42]

	T1w	T2w	FLAIR	T1G	CT
Oligodendroglioma	lower signal intensity than that of the grey matter	hyperintense signal with marked heterogeneity		minimal to moderate patchy, multifocal enhancement in up to 50% of cases	calcifications in the tumor
Anaplastic oligodendroglioma	lower signal intensity than that of the grey matter	hyperintense signal with generally more heterogeneity than oligodendroglioma, peritumoral edema		generally more multifocal enhancement than oligodendroglioma	calcifications in the tumor
Diffuse astrocytoma	iso- or hypointense T1w signal compared to white matter	mass-like T2w hyperintense signal, following white matter more prominent than oligodendroglioma	hypointense FLAIR signal with a rim hyperintensity		
Anaplastic astrocytoma	iso- or hypointense T1w signal compared to white matter	mass-like T2w hyperintense signal, following white matter more prominent than oligodendroglioma	hypointense FLAIR signal with a rim hyperintensity	often enhancement	
Glioblastoma	iso- or hypointense T1w signal compared to white matter	mass-like T2w hyperintense signal with peritumoral edema	mass-like FLAIR hyperintense signal with peritumoral edema	typical ring enhancement with central necrosis	

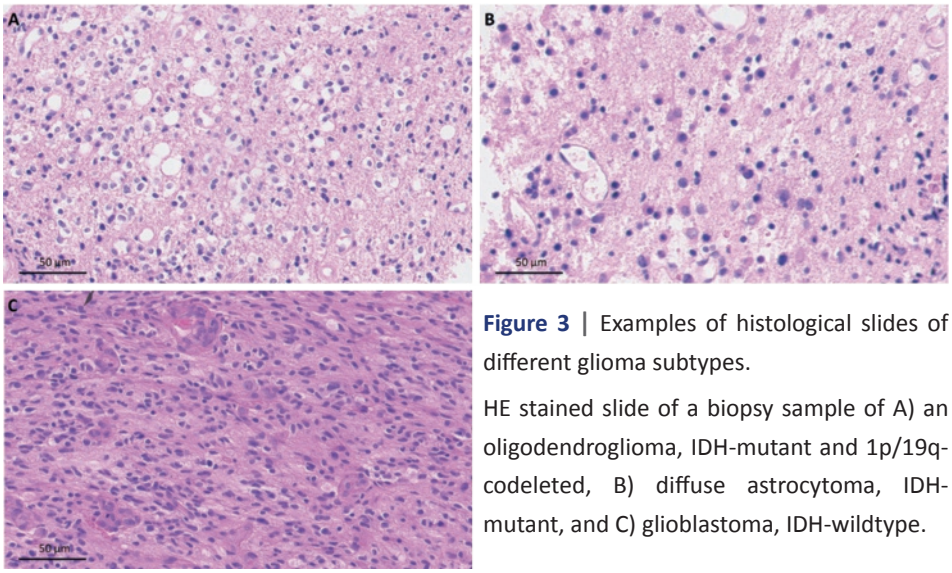

Figure 3 | Examples of histological slides of different glioma subtypes.

HE stained slide of a biopsy sample of A) an oligodendroglioma, IDH-mutant and 1p/19q-codeleted, B) diffuse astrocytoma, IDH-mutant, and C) glioblastoma, IDH-wildtype.

For oligodendroglioma, these characteristics are cytological atypia, possible with limited anaplasia, in WHO grade II and anaplasia and mitotic activity, possible with microvascular proliferation and/or necrosis, in WHO grade III. For astrocytic gliomas, the characteristics are cytological atypia alone in WHO grade II, anaplasia and mitotic activity in WHO grade III and anaplasia and mitotic activity with microvascular proliferation and/or necrosis in WHO grade IV, glioblastoma (Figure3C).[28]

As discussed above, molecular diagnostics include assessment of IDH- 1p/19q- status, and based on combined 'histomolecular' analysis the following main groups of gliomas are recognized; diffuse low grade or anaplastic astrocytoma, IDH-mutant (WHO grade II or III); low grade or anaplastic oligodendroglioma, IDH-mutant and 1p/19q-codeleted (WHO grade II or III); glioblastoma, IDH-mutant (WHO grade IV); diffuse, histologically low grade or anaplastic astrocytoma, IDH-wildtype, in adults often showing molecular characteristics of high-grade (WHO grade IV) malignancy; glioblastoma, IDH-wildtype (Figure 1).[9]

This classification indeed holds important prognostic value and thereby allows for identification of patients with a longer and shorter expected survival. Compared to IDH-wildtype glioblastomas, life expectancy of patients with an IDH-mutant glioblastoma is

somewhat less poor, with the best prognosis for diffuse IDH-mutant 1p/19q-codeleted gliomas.[9]

Treatment

Current standard glioma treatment is multidisciplinary and consists of surgical resection, radiotherapy and systemic chemotherapy. Surgical resection aims at a reliable tissue diagnosis, reducing symptoms by relieving mass effect, and cytoreduction. It is the initial treatment for patients in a good clinical condition or for patients for whom a resection is expected to improve their clinical condition enough to undergo adjuvant treatment. An alternative is a stereotactic biopsy to obtain solely a reliable tissue diagnosis. Complete resection of the MR-imaging abnormalities, T2w or FLAIR in non-enhancing and T1G in enhancing gliomas, is associated with longer overall survival.[8,43]

Radiotherapy is given to the majority of patients, except for low-grade diffuse astrocytoma, IDH-mutant or oligodendroglioma, IDH-mutant and 1p/19q-codeleted patients with favorable prognostic markers: complete resection, age <40 years and without neurological deficits. Radiotherapy aims at local control and is administered in fractions with a total dose of 40–60 Gy, depending on glioma subtype and grade. The target for radiotherapy is based on three tumor volumes: gross (GTV), clinical (CTV) and planning (PTV). For contrast-enhancing glioma, the GTV includes the resection cavity and residual tumor on T1G MRI. By adding a uniform margin of 20mm to the GTV, to include microscopic spread, the CTV is generated. If T2/FLAIR abnormalities extend beyond this margin, they are to be added to the CTV. Finally, the PTV is generated by adding a 3-5mm margin to the CTV to correct for planning uncertainties originating from patient setup and fusion of the images.[44] For non-enhancing glioma, the GTV includes the resection cavity and abnormalities on T2 or FLAIR MRI. A 15–20mm margin is added for the CTV and another 5–7mm margin for the PTV.[45] Older patients and those with poor performance status receive a hypo-fractionated scheme with a higher fraction dose and lower total dose.[43] Radiotherapy prolongs progression free survival in low-grade glioma patients without favorable prognostic markers,[46] and increases survival in glioblastoma.[47]

Systemic chemotherapy is also given to most glioma patients, except for the low-grade diffuse astrocytoma, IDH-mutant or oligodendroglioma, IDH-mutant and 1p/19q-codeleted patients with favorable prognostic markers. Cytotoxic chemotherapy is administrated for six cycles, starting during radiotherapy, with the agent depending on the glioma subtype. In diffuse and anaplastic oligodendroglioma, a combination of procarbazine,

lomustine and vincristine (PCV) is given, while temozolomide is administrated in diffuse and anaplastic astrocytoma, as well as glioblastoma. Chemotherapy prolongs survival in low-grade glioma and increases survival in glioblastoma.[48,49]

DETECTION OF THE EXTENT OF GLIOMA INFILTRATION

Detection of the extent of glioma infiltration is indispensable for the guidance of surgical resection and radiotherapy. For neurosurgeons, identification of this extent during surgery is difficult due to the diffuse infiltration of glioma into normal brain tissue. The core of the tumor, consisting of densely packed tumor cells and necrosis, is fairly recognizable under the operating microscope, but peripheral infiltration, extending beyond tumor cavity margins and consisting of more preexisting brain tissue than tumor cells, however, is virtually impossible as it looks and feels like normal brain. Recently, fluorescence guidance has been introduced in glioma surgery to help identify the tumor.[50] Although a promising technique, a randomized clinical trial only demonstrated its benefit to increase the resection percentage of the tumor core, as defined on imaging, and not the infiltration outside the core.[50] Also, multiple studies found imaging more sensitive for the detection of glioma infiltration than fluorescence.[51,52] Therefore, in daily practice, both neurosurgeons and radiation oncologists use various imaging modalities and MRI sequences to detect the extent of glioma infiltration.

Current standard MRI sequences for detection of glioma infiltration

Different imaging modalities are available for glioma imaging, with MRI currently being recommended as standard. [38] T2w, FLAIR and T1G MRI are currently used in daily practice for the delineation of gliomas.

In enhancing gliomas, T1G MRI is used to guide local treatment. The basic principle of T1G MRI is the intravenous administration of a gadolinium-based contrast agent with paramagnetic properties, which allows for clear visualization of vascular structures. Due to the disruption of the BBB by a glioma, contrast will leak outside vascular structures resulting in parenchymal enhancement. This enhancement allows for clear delineation of the regions of the tumor with BBB breakdown. Other regions of the tumor, however, do not display BBB breakdown and will therefore not enhance on T1G MRI. This has been

confirmed by multiple studies that demonstrated the presence of glioma infiltration outside regions with enhancement on T1G MRI.[51-69]

In non-enhancing gliomas, T2w or FLAIR MRI is used for treatment guidance. The hyperintense T2w signal of a non-enhancing glioma depends on the increase of extracellular fluid, which can be caused by edema, myelin loss and other damage to central nervous system tissue.[70] FLAIR is a T2-weighted sequence with suppression of the hyperintense signal of the cerebrospinal fluid, resulting in improved identification of signal changes in the periventricular regions and periphery of the hemispheres. As with T1G MRI, glioma infiltration has been demonstrated outside imaging abnormalities on both T2w and FLAIR MRI.[4] Vice versa, samples from T2w hyperintense regions in patients with non-enhancing glioma not necessarily show tumor presence.[71]

Alternative MRI sequences and imaging modalities for detection of glioma infiltration

Besides T2w, FLAIR and T1G MRI, other MRI sequences are available for the detection of glioma infiltration. These include DWI, diffusion tensor imaging (DTI), perfusion-weighted imaging (PWI) and magnetic resonance spectroscopy imaging (MRSI). Examples of these sequences are presented in Figure 4A.

DWI is included in the standard MRI protocol, however, primarily to detect ischemia after surgical resection instead of glioma infiltration detection. The basics of DWI is the Brownian movement of hydrogen molecules in their surroundings, so-called diffusion, where restricted diffusion results in a low and free diffusion in a high signal. Since diffusion imaging also incorporates T2w signals, the Apparent Diffusion Coefficient (ADC) is used to eliminate these T2w signals. ADC appears to correlate with cellularity in glioma,[72] although contradicting results have been reported.[73]

Figure 4 | Examples of alternative imaging.

A) Exemplary MRI sequences of a left parietal glioblastoma, IDH-wildtype. B) *Left:* CT of a left parietal glioblastoma, IDH-wildtype , *center:* intraoperative ultrasound and *right*: [^{11}C]choline and [^{18}F]FET PET of a left parietal glioblastoma, IDH-wildtype. ADC =Apparent Diffusion Coefficient, FA =fractional anisotropy, ASL-CBF =Arterial Spin Labeling Cerebral Blood Flow, DSC-CBV =Dynamic Susceptibility Contrast Cerebral Blood Volume, MRSI-CNI =Magnetic Resonance Imaging Spectroscopy Cho to NAA index, CT =computational tomography, PET =positron emission tomography and FET =O-(2-[18F]-fluoroethyl)-L-tyrosine

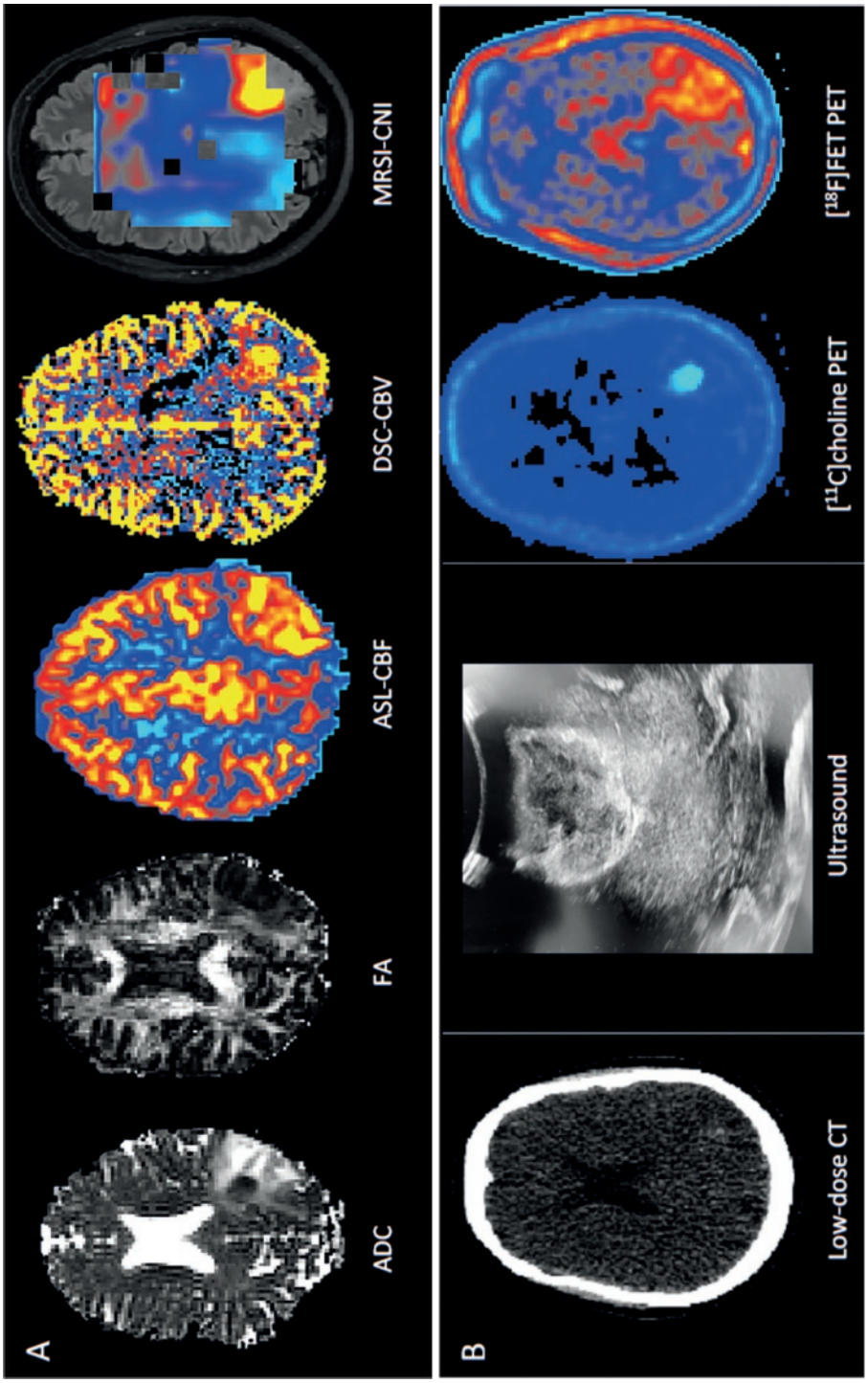
A
ADC
FA
ASL-CBF
DSC-CBV
MRSI-CNI
B
Low-dose CT
Ultrasound
[11C]choline PET
[18F]FET PET

DTI is another diffusion-based technique, which measures the direction, instead of the magnitude, of diffusion. The strictness of the direction varies from completely rigid to completely free and is assessed with the metric fractional anisotropy (FA). This is especially useful for the visualization of the white matter tracts. Since glioma infiltration tends to follow the white matter tracts, disruption of the FA signal in a tract is indicative for tumor presence.[74]

PWI measures the perfusion of tissue by blood. The two most used metrics are cerebral blood flow (CBF) and volume (CBV). CBF is defined as the volume of blood passing through a given amount of brain tissue per unit of time and CBV as the volume of blood present in a given amount of brain tissue.[75] Three MRI perfusion techniques are available, of which dynamic susceptibility contrast (DSC) and dynamic contrast-enhanced (DCE) are based on the administration of contrast, while arterial spin labeling (ASL) uses hydrogen atoms in the supplying arteries to the brain as a contrast agent and can only be used to assess CBF. PWI metrics, especially CBV, are correlated with angiogenesis and histological WHO grade in glioma.[76]

MRSI measures the biochemical components of a region of interest, providing information on the concentration of multiple metabolites. The metabolite N-acetyl aspartate (NAA), synthesized by normal neurons and therefore decreased in gliomas,[77] and total-choline-containing metabolites (Cho), increased in gliomas due to the breakdown of cell membranes,[78] are used to calculate the Cho to NAA index (CNI). CNI-based volumes have been used to guide glioma surgery in a single study.[79]

Next to MRI, other imaging modalities such as computed tomography (CT), ultrasound and positron emission tomography (PET) have been used for glioma delineation. Examples of these modalities are presented in Figure 4B.

CT combines multiple X-rays from different angles to produce an image. It was introduced in the 1970s and was the first 3D imaging modality used for the resection of gliomas.[80] It is still used in emergency settings but MRI has replaced it as the standard imaging modality.

Ultrasound uses high frequency sound waves and the acoustic properties of tissue, namely absorption, scattering or reflection, to visualize tissue. Since sound waves are almost completely reflected by bone, in glioma patients ultrasound is generally used intraoperatively after the craniotomy. A major advantage compared to other imaging

techniques is that these images are real-time instead of pre-operative acquired. Glioma tissue produces a hyperechoic signal due to the relative high mass density of the tissue. This allows for discrimination with normal brain tissue, which is iso-echogenic, resulting in a white tumor signal between gray normal brain.[81]

PET is an imaging technique that measures the radioactivity of intravenously administrated radioactive tracers. These tracers are biological compounds with an attached radioactive label. Different biological compounds and labels are available. The compound, generally, determines the distribution of the traces in different tissues, while the type of label determines the duration of the radioactive signal. Multiple tracers are used in glioma imaging, of which glucose and the amino acids O-(2-[18F]-fluoroethyl)-L-tyrosine ([^{18}F]FET) and L-[methyl-11C]methionine ([^{11}C]MET) are most widely used and studied.[82] Recently, the Response Assessment in Neuro Oncology workgroup has recommended the use of amino acid PET as standard for the delineation of glioma.[83,84]

Neuronavigation

Once glioma infiltration is detected on imaging, accurate localization in the patient during treatment is realized with neuronavigation, a technique that uses a high-resolution image, CT or MRI, to produce a 3D model of the patient's head. In the operation or radiotherapy room a virtual 3D environment is created using a reference star indirectly attached to the patient. With an optical or electromagnetic tracking system, anatomical landmarks on the patient's head are spatially registered in the 3D environment to match the 3D model of the patient's head.[85] After this registration, the position of a probe, surgical tool, microscope or radiation device in relation to the reference star can be determined in the 3D model. By correlating imaging sequences to the one used for the 3D model, the 3D position is translated to all imaging sequences. An example of a neuronavigation setup is presented in Figure 5.

A limitation of this technique is the possible inaccuracy in spatial registration that can occur at the different steps of the process. Imperfect correlation of image sequences, a noisy 3D imaging model of the head, inaccurate identification of anatomical landmarks and the movement of the reference point in relation to the patient can all lower the registration accuracy.[86] Another limitation is the brain shift that occurs after opening of the dura and resection of tissue. Since the 3D model was based on preoperative imaging, this shift cannot be incorporated into the navigation, thus resulting in lower accuracies during the progress of the surgical resection.

Figure 5 | Example of a frameless neuro-navigation setup.

1) Patient fixated in a head clamp. 2) Reference star attached to the head clamp. 3) Neurosurgeon identifying anatomical landmarks on patient with navigated pointer. 4) Optical tracking system aimed at the patient's face and reference star. 5) Neuronavigation station.

Assessment of the accuracy of imaging to detect glioma infiltration

In order to compare the different imaging techniques for their ability to detect glioma infiltration, an objective quantitative metric is necessary. Diagnostic accuracy is the ability of an index test to classify an element into one of two conditions. In order to compare the index test with the 'truth', a reference test, preferably the current gold standard, is used to classify an element as with or without the condition. The classification of the index test is subsequently compared with the classification of the reference test. In this thesis, the index test is an imaging technique, while the reference test is the histopathological assessment of tumor presence in a sample from a glioma patient. The comparison of the index and reference test results in a two-by-two table (Table 2).

Table 2 | Diagnostic accuracy two-by-two table.

	Condition present	Condition absent
Index test positive	True Positive (TP)	False Positive (FP)
Index test negative	False Negative (FN)	True Negative (FN)

Different diagnostic accuracy metrics are available, of which we will discuss sensitivity and specificity. Sensitivity is the ratio between the true positives and the total number of samples with the condition, which are the true positives and false negatives together (TP/(TP+FN)). An index test with a high sensitivity is good in determining if the condition is present in a sample with the condition. In this thesis, this would result in few samples with tumor presence being classified as normal. Specificity is the ratio between the true negatives and the total number of elements without the condition, which are the true negatives and false positives together (TN/(TN+FP)). An index test with a high specificity is good in determining if the condition is not present in an element without condition. In this thesis, this would result in few samples without tumor presence being classified as tumor.

The index test's discrimination between the two conditions can depend on the interpreter of the index test in case of a qualitative test or the threshold in a quantitative test. For each interpreter or threshold, a new two-by-two table can be conducted with a corresponding sensitivity and specificity. These sensitivities and specificities can be plotted in a graph with 1-specificity on the x-axis and sensitivity on the y-axis. This graph is called a receiver operating characteristic (ROC) curve (Figure 6). If using a toss coin, the curve would be a diagonal line from the bottom left to the top right. For a perfect test, the curve would follow the left and top border. The ROC curve can be used to determine the optimal threshold, depending on the definition of optimal, such as the highest sum of sensitivity and specificity. The area under the ROC curve (AUC) is a metric that represents the overall performance, also called diagnostic accuracy, of an index test, with an AUC of 0.5 for the toss coin and 1.0 for the perfect test.

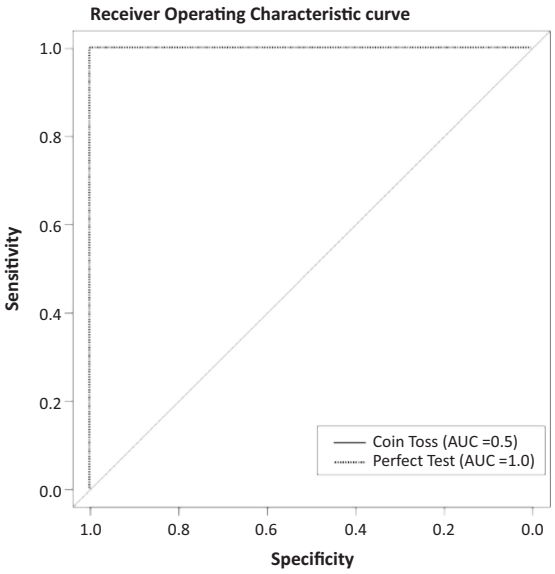

Figure 6 | Example of a Receiver Operating Characteristic curve.
ROC curve, with 1-specificity on the x-axis and sensitivity on the y-axis, with the toss coin curve (black line) and perfect test curve (dashed line) and their corresponding areas under the ROC curve (AUC).

CURRENT PROBLEM

As discussed above, the accuracy of current standard MRI for the detection of extent of glioma infiltration is quite limited. More accurate MRI sequences and/or imaging modalities are necessary to improve glioma delineation so local treatment can be guided beyond the current MRI abnormalities, as well as to identify patients with glioma infiltration beyond meaningful local treatment to avoid futile treatment.

AIMS OF THIS THESIS

The studies in this thesis aim to identify the optimal MRI sequence, PET tracer, or combination of MRI sequence(s) and/or PET tracer(s) for the detection of glioma infiltration. The overall objectives were the following:

- To discuss the current literature concerning imaging for the detection of extent of glioma infiltration
- To develop quantitative [^{18}F]FET PET parametric maps
- To compare the accuracy of different MRI sequences, PET tracers and combinations of MRI sequence(s) and/or PET tracer(s) for the detection of extent of glioma infiltration
- To quantify glioma infiltration using histological, molecular and imaging techniques

OUTLINE OF THIS THESIS

Chapter 2 presents a meta-analysis concerning studies that addressed the diagnostic accuracy of pre-operative imaging to delineate gliomas using direct comparison with histopathology. In **Chapter 3** the literature is reviewed for imaging techniques used for glioma delineation and localization of brain functions. The way in which these techniques can be used to achieve a maximal safe resection is discussed. In **Chapter 4** the accuracy of the frameless stereotactic drilling technique is assessed, by comparing post-operative depth-electrode position with pre-operative planning. This biopsy technique is used in chapters 8-10. **Chapter 5** describes the protocol of the prospective study described in chapters 6-10. In **Chapter 6** the optimal metabolite-corrected plasma input model is identified for the quantification of [^{18}F]FET kinetics. Reference tissue input models and simplified methods are validated with the full kinetic analysis results. Using these models, the accuracy of parametric images and tumor-to-normal maps for quantifying [^{18}F]FET uptake is determined in **Chapter 7**. With these parametric images and tumor-to-normal maps, the diagnostic accuracy of [^{11}C]choline and [^{18}F]FET PET to detect the extent of glioma infiltration is directly compared in **Chapter 8**. **Chapter 9** presents the results of the direct comparison of diagnostic accuracy of multiple MRI sequences, PET tracers and combinations of MRI sequence(s) and/or PET tracer(s) for the detection of extent of glioma infiltration. **Chapter 10** describes the quantitative analysis of tumor purity using histological, molecular and imaging techniques and the influence of tumor purity on intratumoral genetic heterogeneity. Finally, the general discussion is presented in **Chapter 11** and remaining challenges and future directions in the field are discussed.

Niels Verburg
Friso W.A. Hoefnagels
Frederik Barkhof
Ronald Boellaard
Serge Goldman
Jun Guo
Jan J. Heimans
Otto S. Hoekstra
Rajan Jain
Manabu Kinoshita
Petra J.W. Pouwels
Stephen J. Price
Jaap C. Reijneveld
Andreas Stadlbauer
W. Peter Vandertop
Pieter Wesseling
Aeilko H. Zwinderman
Philip C. De Witt Hamer

Am J Neuroradiol 2017 Oct;38(10):1884-1891

Chapter 2

Diagnostic accuracy of neuroimaging to delineate diffuse gliomas within the brain: a meta-analysis

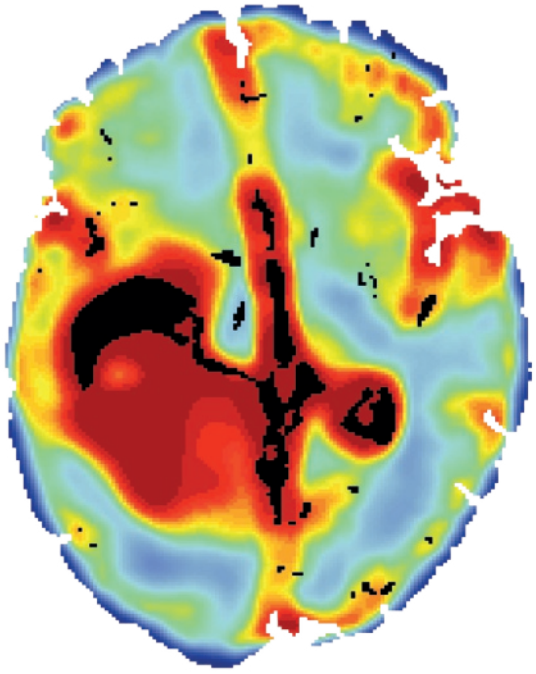

ABSTRACT

Background: Brain imaging in diffuse glioma is used for diagnosis, treatment planning, and follow-up.

Purpose: In this meta-analysis, we address the diagnostic accuracy of imaging to delineate diffuse glioma.

Data Sources: We systematically searched studies in adults with diffuse glioma and correlation of imaging with histopathology.

Study selection: Study inclusion was based on quality criteria. Individual patient data was used, if available.

Data analysis: A hierarchical summary ROC method was applied. Low- and high-grade gliomas were analyzed in subgroups.

Data Synthesis: 61 studies described 3,532 samples in 1,309 patients. The mean STARD score (13/25) indicated suboptimal reporting quality. For diffuse glioma as a whole, the diagnostic accuracy was best using T2-weighted MRI, measured as area under the curve, false positive rate, true positive rate and diagnostic odd ratio of 95.6%, 3.3%, 82%, and 152. For low-grade glioma, the diagnostic accuracy of T2-weighted MRI as reference was 89.0%, 0.4%, 44.7%, and 205; and for high-grade glioma of T1-weighted gadolinium-enhanced MRI as reference: 80.7%, 16.8%, 73.3%, and 14.8. In high-grade gliomas, MR spectroscopy (85.7%, 35.0%, 85.7%, and 12.4) and MET PET (85.1%, 38.7%, 93.7%, and 26.6) performed better than reference imaging.

Limitations: True negative samples were underrepresented in this data, so that false positive rates are probably less reliable than true positive rates. Multimodality imaging data was unavailable.

Conclusion: The diagnostic accuracy of commonly-used imaging for delineation is better for low-grade glioma than for high-grade glioma based on limited evidence. Improvement is indicated from advanced techniques, such as MR-spectroscopy and PET.

INTRODUCTION

Diffuse gliomas are the most common primary brain tumors in adults with an annual incidence of approximately 6 per 100,000. Despite advances in neurosurgery, radiotherapy, and chemotherapy, gliomas are fatal.[87] Brain imaging is indispensable for the diagnosis, treatment planning and evaluation, and follow-up. Although imaging standards to plan resection and radiotherapy vary between institutions and specialists, conventional imaging is in common use, typically consisting of T1-weighted MRI before and after gadolinium and T2/FLAIR-weighted MRI for gliomas. Of these conventional sequences, T2/FLAIR-weighted MRI is often considered as reference for low-grade gliomas, and T1-weighted gadolinium-enhanced MRI for high-grade gliomas in neuro-surgical planning, combined with T2-weighted MRI in radiotherapy planning.[88,89]

Compared to other cancer types, accurate delineation of glioma within the brain for treatment planning is particularly important due to the proximity of eloquent brain structures, that are vulnerable to surgery and radiotherapy.[90] Conversely, more extensive resections and boosted radiotherapy correlate with longer survival.[91-93] At the same time, clinical observations challenge the diagnostic accuracy of current imaging protocols: gliomas recur even after a radiologically complete resection[8,94] and glioma cells were detected outside MRI abnormalities[3,54] Brain imaging techniques, such as multivoxel spectroscopy and PET were developed to improve tumor grading and delineation.[95,96]

Inherent to any regional treatment, such as surgery and radiotherapy, is the need to delineate a target volume, which mandates a dichotomous classification into tumor and normal tissue. Low-grade and high-grade gliomas have different treatment strategies and prognosis, while both are characterized by diffuse tumor infiltration. This grounds our pooled analysis for diffuse glioma in addition to subgroup analysis by glioma grade. More accurate glioma delineation may improve the consistency between treatment results and survival. For instance, more accurate delineation may serve to identify patients eligible for more aggressive surgery than would have been considered based on conventional imaging, as well as to identify patients with glioma infiltration beyond meaningful surgical therapy, so that useless, and possibly harmful, resections can be avoided.

The diagnostic accuracy of imaging techniques to delineate gliomas has not been systematically addressed. In this meta-analysis we estimate and compare the diagnostic

accuracies of conventional imaging techniques and advanced MRI and PET to delineate newly-diagnosed diffuse glioma within brain tissue in adults.

MATERIALS AND METHODS

Search strategy

We aimed to identify all publications reporting glioma imaging correlated with histopathology for the sampled locations. Our data sources were the National Library of Medicine (PubMed/MEDLINE, beginning in 1966) and the Excerpta Medica Database (EMBASE, beginning in 1947), accessed on February 29, 2016, searching MESH and EMTREE subject headings (Supplemental Methods 1). The publication language was restricted to western languages; the publication date was restricted until January 1, 2016. References of identified studies were reviewed for further eligible publications in adherence with the PRISMA statement guidelines (Supplemental Table 1).

Study selection criteria

Studies were eligible for further analysis based on five inclusion criteria. First, an adult (sub-)population was required with patients at least 18 years of age. Second, only newly-diagnosed diffuse glioma of World Health Organization (WHO) grade II-IV was included to avoid imaging artifacts from previous treatment. Third, brain imaging of any technique was allowed as diagnostic test. Fourth, histopathology of tissue samples was required as reference test. Fifth, the histopathology of samples and imaging test measurements had to be directly correlated by surgical navigation using 3D-coordinates. When duplicate reports on the same population were retrieved, only the report with the most complete data was used for analysis. Studies also including patients of pediatric age or pathology other than diffuse glioma were included if the population of interest could be extracted from the data. Postmortem studies were excluded to avoid bias from end-stage disease. For interobserver agreement on study inclusion, a kappa statistic was used.[97]

Quality and outcome measures

Any study reporting glioma imaging correlated with histopathology was independently assessed in full-text for quality criteria by two observers (NV and FH, with three and eight years of experience in clinical neurosurgery) using the Standard for Reporting of Diagnostic Accuracy (STARD) guidelines, a 25 item checklist to explore reporting quality.[98] Disagreements were resolved through adjudication by a third observer (PWH, with 15

years of experience in clinical neurosurgery). For interobserver agreement on quality assessment, the intra-class correlation coefficient was calculated. One observer extracted the study data (NV) on the imaging techniques, the histopathological examination method, the co-localization method between imaging and histopathology, and the number of patients and samples categorized by glioma grades. The extracted data was verified by another observer (PWH). Biopsy sample locations were categorized for each imaging technique as normal or abnormal signal according to the authors' test positivity criteria, and as glioma or normal brain in correlated histopathological examination according to the authors' definitions. We aimed to include individual sample data as much as possible, either by availability from the publication, by request for original data to corresponding authors (up to three times in case of non-response), or by estimation of data points from plots of image measurements versus tumor characteristics. If individual sample data was unavailable, we included the aggregated data as summaries of true positive (TP), true negative (TN), false positive (FP), and false negative (FN) samples. Accordingly, each imaging technique in every study provided at least one estimate of diagnostic accuracy.

Statistical analysis

We used hierarchical summary receiver operating characteristic (hsROC) curve analysis with random-effects for within-study and between-studies variation to summarize estimates of the diagnostic accuracy for each imaging technique with more than one study available (Supplemental Methods 2).[99] The available data allowed for hierarchical analysis of samples within techniques. The estimates with 95% credibility intervals (CI) consisted of the summary true positive rate (sensitivity: TP/[TP+FN]), the summary false positive rate (1-specificity: FP/[FP+TN]), the diagnostic odds ratio ([TP/FN]/[FP/TN]),[100] and the summary area under the ROC curve. Differences in estimates between imaging techniques in relation to reference imaging were also calculated and considered significant when the CI excluded zero. A Bayesian Markov Chain Monte Carlo algorithm using three chains modeled the hsROC curve with CI for each imaging technique based on five parameters: the accuracy and its precision, the cutpoint and its precision, and the scale parameter.[101] The accuracy and the cutpoint were allowed to vary between studies; the scale was allowed to vary between imaging techniques. These parameters provide an hsROC curve with an operating point on the curve representing the summary true positive rate and summary false positive rate. A Bayesian hsROC analysis was used for the following reasons. First, this approach is considered the standard for meta-analysis of diagnostic accuracy taking into account the correlation between the true positive

rate and false positive rate.[101,102] Second, individual sample data and aggregated data, if individual data is unavailable, can be analyzed together per imaging technique to estimate its diagnostic accuracy.[103,104] Third, varying test positivity criteria for imaging in studies can be accommodated.[105] Fourth, partly missing data can be handled using this model. For the meta-analysis, vague priors were chosen for the prior distributions, so that the results primarily reflect inference from the presented data without prior knowledge. Normal distributions with mean 0 and variance 10,000 represented the accuracy, cutpoint and scale parameters, and inverse gamma distributions with a shape and rate of 0.01 represented the precisions. Uniform distributions were used as alternative vague priors. Summary estimates consisted of the median values with CI of the posterior distributions. For the analysis we used JAGS software, version 4.0.1 (Jags Software, Newark, DE; http://mcmc-jags.sourceforge.net) called from the rjags package (version 4-3) for R (version 3.2.2; R Foundation for Statistical Computing, Vienna, Austria; http://www.R-project.org). Sampling traces and distributions, and Gelman-Rubin diagnostics were evaluated for evidence against convergence using the coda package (version 0.17.1). Statistical tests for heterogeneity between studies are unavailable for diagnostic accuracy meta-analysis, therefore heterogeneity was explored using subgroup analysis.[106] Sensitivity analysis included analysis of (a) the subset of higher-quality studies, considered those with a prospective design, including quantified sample data in at least 15 patients, and qualifying for the methodological description of both neuro-imaging and histopathology,[107] (b) the subset of studies with individual patient data, and (c) alternative vague prior distributions. Subgroups of low-grade (WHO grade II) and high-grade glioma (WHO grade III or IV) were reported separately. Publication bias was explored graphically.

RESULTS

The search strategy identified 8,558 unique citations (Figure 1), of which 272 full-text publications were assessed for eligibility. Subsequently, 61 articles were included for meta-analysis based on the five selection criteria. The interobserver agreement for inclusion was moderate (kappa 0.47, 95%CI: 0.37–0.57). A total of 3,532 samples with correlated histopathological examination and imaging were included from 1,309 patients with a glioma. For subgroup analysis by glioma grade, data could be extracted for 907 samples in 421 patients with low-grade glioma, and for 1,380 samples in 814 patients with high-grade glioma. Glioma subtypes, such as astrocytoma or oligodendroglioma,

could not be analyzed in subgroups, because data for these subgroups could usually not be extracted. Individual sample data were available from 19 studies. The higher-quality subset consisted of 29 studies.

The mean STARD score of the included studies was 13 (s.d. 2.8). The interobserver agreement for STARD quality assessment was substantial (intra-class coefficient: 0.66, 95%CI: 0.49–0.78).

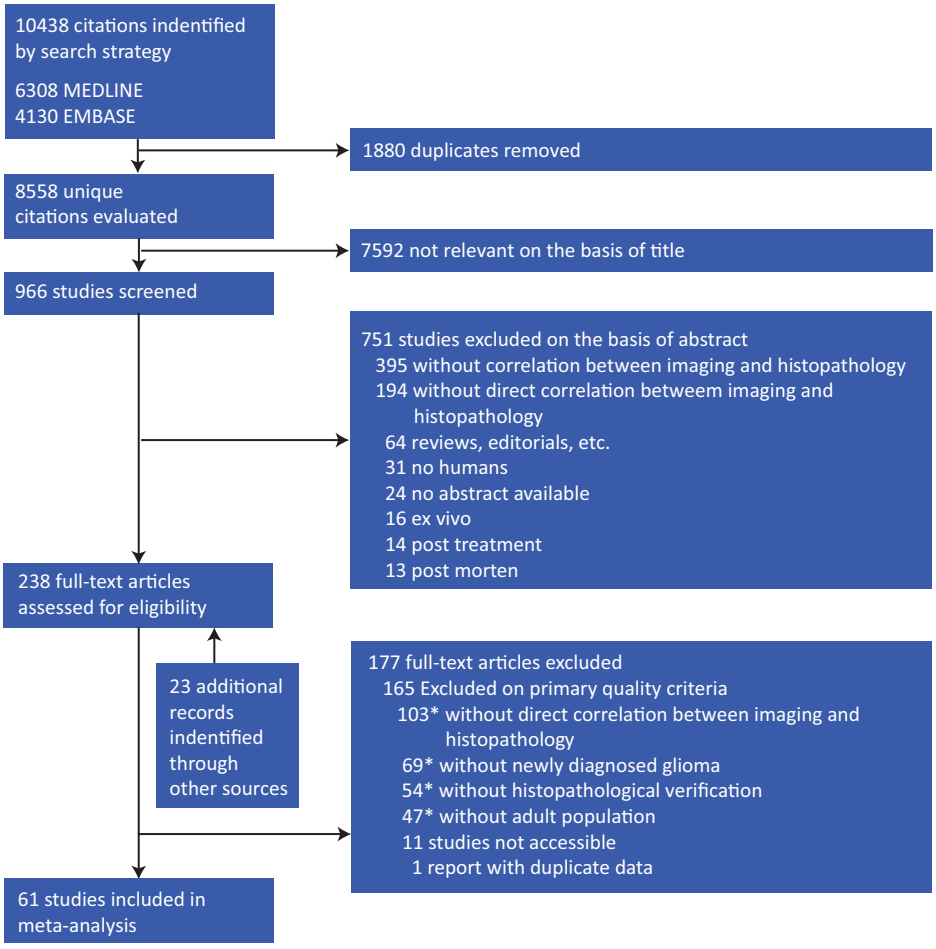

Figure 1 | Flow chart of publication selection. * Multiple exclusion criteria could apply to studies.

The included studies reported on 16 imaging techniques, including T1-weighted MRI before and after gadolinium, T2-, T2/FLAIR-, perfusion-, diffusion-weighted MRI (apparent diffusion coefficient), MRI spectroscopy (choline to N-acetyl aspartate ratio), MR diffusion tensor imaging (fractional anisotropy), and PET imaging with these tracers: [18F-]fluorodeoxyglucose (FDG), [11C-]methionine (MET), [18F-]fluoroethyltyrosine (FET), [18F-]fluorthymidine (FLT), or [18F- or 11C-]choline (CHO). Imaging protocols varied widely, for instance 22 studies used 1.5-T MRI field strength, 15 used 3.0-T, one used 0.15-T, and field strength was unspecified in 11 studies. The number of studies, patients, and samples for each imaging technique categorized by glioma grades is plotted in Figure 2.

The reference standard to distinguish tumor and normal brain in tissue samples for all studies was microscopic examination using hematoxylin/eosin staining and immunohistochemical analysis. Nine studies reported the reference standard as labeling index of proliferating cells, six studies reported the reference standard as tumor infiltration index and two studies as cellularity index. We followed the authors' definition to differentiate normal brain and glioma.

The method to correlate the histopathology with imaging was frameless stereotactic needle biopsies in 27 studies, frame-based stereotactic needle biopsies in 14, neuronavigated resection biopsies in 12, and unspecified stereotactic needle biopsies in eight.

The hsROC curves of imaging techniques for diffuse glioma as a whole are plotted in Figure 3A, and for the subgroups of low- and high-grade glioma in Figures 3B and 3C, respectively. The characteristics of these hsROC curves are listed in Figure 4.

Estimated summary ROC curves are plotted by imaging technique in ROC space for diffuse glioma as a whole, i.e. low- and high-grade glioma combined, in 3A, low-grade glioma in 3B, and high-grade glioma in 3C. The operating points of curves represent the estimated summary true positive and false positive rates as indicated by solid squares. Solid squares are missing when convergence was not reached. Color coding as in the legend, with conventional MRI in black, advanced MRI in shades of blue, PET imaging in shades of red, and CT and ultrasound imaging in shades of green.

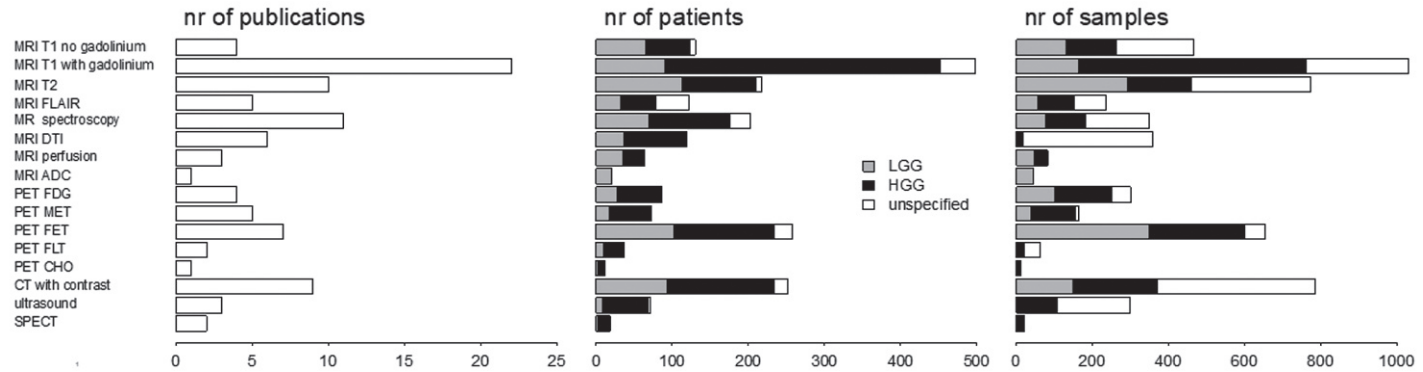

Figure 2 | Number of publications, patients and samples for imaging techniques categorized by glioma grade

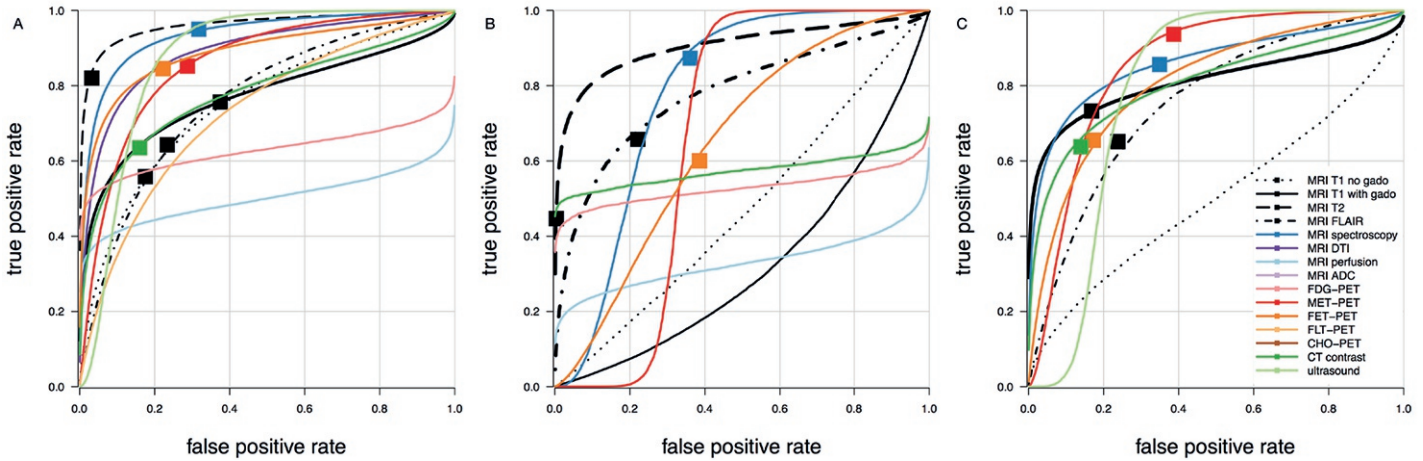

Figure 3 | Summary hierarchical ROC curves of imaging techniques.

A
Modality
Nr papers
Nr patients
Nr samples
Area under summary ROC curve (95% c.i.)
Summary false positive rate (95% c.i.)
Summary true positive rate (95% c.i.)
Diagnostic odds ratio (95% c.i.)
MRI T1–
MRI T1+
MRI T2
MRI flair
MRI spectro
MRI dti fa
MRI pwi
MRI ADC
PET Mg
PET met
PET fet
PET fl
PET cho
CT
Ultrasound
SPECT
B
Modality
Nr papers
Nr patients
Nr samples
Area under summary ROC curve (95% c.i.)
Summary false positive rate (95% c.i.)
Summary true positive rate (95% c.i.)
Diagnostic odds ratio (95% c.i.)
MRI T1–
MRI T1+
MRI T2
MRI flair
MRI spectro
MRI dti fa
MRI pwi
MRI ADC
PET Mg
PET met
PET fet
PET fl
PET cho
CT
SPECT
C
Modality
Nr papers
Nr patients
Nr samples
Area under summary ROC curve (95% c.i.)
Summary false positive rate (95% c.i.)
Summary true positive rate (95% c.i.)
Diagnostic odds ratio (95% c.i.)
MRI T1–
MRI T1+
MRI T2
MRI flair
MRI spectro
MRI dti fa
MRI pwi
PET Mg
PET met
PET fet
PET fl
PET cho
CT
Ultrasound
SPECT

Figure 4 | Diagnostic accuracy characteristics of imaging techniques.

Diagnostic performance of imaging techniques expressed as area under the curve, summary false positive rate, summary true positive rate, and diagnostic odds ratio for diffuse glioma as a whole, i.e. low- and high-grade glioma combined, in 4A, low-grade glioma in 4B, and high-grade glioma in 4C. The medians of posterior distributions is plotted as squares proportional to the number of observations with 95% credibility intervals. The most common clinically utilized imaging technique is printed in blue as reference. n.a. represents non-available data because either less than three studies were available or the posterior samples did not converge.

In particular the estimates of false positive rates need to be interpreted with significant caution due to relative lack of data on true negative samples (Supplemental data). This "underrepresentation" of true negatives and consequently bias in false positive rates may be unbalanced across imaging techniques, creating additional biases when comparing the ROC curves.

All gliomas considered, the area under the curve was highest for T2-weighted MRI (95.6%), followed by MRI spectroscopy (93.3%). The false positive rate was lowest in T2-weighted MRI (3.3%), followed by CT (16.0%), and the true positive rate was highest for MRI spectroscopy (95.0%), followed by ultrasound (93.3%). The diagnostic odds ratio was highest for T2-weighted MRI (152), followed by MRI spectroscopy (39.2).

For low-grade gliomas, the area under the curve was highest for T2-weighted MRI (89.0%), followed by MRI spectroscopy (78.1%) and T2/FLAIR-weighted MRI (77.4%). The false positive rate was lowest in T2-weighted MRI (0.4%), followed by T2/FLAIR-weighted MRI (22.1%), and the true positive rate was highest for MRI spectroscopy (87.3%), followed by T2/FLAIR-weighted MRI (65.8%). The diagnostic odds ratio was highest for T2-weighted MRI (205), followed by MRI spectroscopy (15.7). Unsurprisingly, the area under the curve was statistically significantly lower for T1-weighted gadolinium-enhanced MRI compared with T2-weighted MRI (difference of 54.4%, CI: 8.4–80.8%), and for perfusion-weighted MRI (difference of 54.1%, CI: 7.8–78.2%). Of note, T2-weighted MRI had a higher area under the curve, false positive ratio and diagnostic odds ratio in comparison with T2/FLAIR-weighted MRI, the other common clinically utilized MRI sequence.

For high-grade gliomas, the area under the curve was highest for MRI spectroscopy (85.7%), followed by MET-PET (85.1%). The false positive rate was lowest in CT (14.0%),

followed by T1-weighted gadolinium-enhanced MRI (16.8%), and the true positive rate was highest for MET-PET (93.7%), followed by MRI spectroscopy (85.7%). The diagnostic odds ratio was highest for MET-PET (26.6), followed by T1-weighted gadolinium-enhanced MRI (14.8). MET-PET and MR spectroscopy had a higher area under the curve and true positive rate in comparison with the common clinically utilized T1-weighted gadolinium-enhanced MRI (respectively 80.7% and 73.3%). This came at the expense of higher false positive rates for MET-PET and MR spectroscopy, respectively 38.7% and 35.0%. Remarkably, CT with contrast had an area under the curve (80.0%) similar to T1-weighted gadolinium-enhanced MRI.

Sensitivity analysis demonstrated robustness against publication quality, individual sample data, and alternative vague priors (Supplemental Figure 1). As statistical tests for heterogeneity are unavailable to take the association between sensitivity and specificity into account,[106] we inspected the plots of study data and hsROC curve for each technique (Supplemental Figure 2), demonstrating considerable heterogeneity between studies, resulting in relatively large CI. For many imaging techniques the number of publications is too small to exclude publication bias (Supplemental Figure 3). Small studies with small areas under the curve or low false positive rates may be missing for T1-weighted gadolinium-enhanced MRI and T2-weighted MRI.

DISCUSSION

The main findings of this meta-analysis are that the diagnostic accuracy of neuro-imaging to delineate diffuse glioma a) is best using T2-weighted MRI, followed by MR spectroscopy, b) is better for low-grade glioma using T2-weighted MRI, than for high-grade glioma using T1-weighted gadolinium-enhanced MRI, considering the area-under-the-curve (89.0% versus 80.7%) and the diagnostic odds ratio (205 versus 14.8), c) may be improved in high-grade glioma by MR spectroscopy or MET-PET, d) is not superior using T2/FLAIR-weighted MRI for low-grade glioma, e) is not inferior by CT with contrast for high-grade glioma, and f) varies considerably between imaging techniques and shows heterogeneity between studies.

Thresholds for acceptable diagnostic accuracy of tumor imaging are undetermined. The accuracy of imaging for glioma delineation by MRI is, for instance, less than lesion detection in hepatocellular carcinoma by ultrasound, CT or MRI.[108] It is comparable with

detection of metastatic lymph nodes in non-small cell lung cancer by CT or MRI, but less than PET.[109,110] And, it is less than the diagnosis of breast cancer by MRI.[111] These studies, however, rather address the radiological diagnosis of cancer by imaging, and not the delineation of infiltrative cancer within normal tissue. The identification of cancer cells within normal appearing imaging regions seems to be specific for glioma.[4,112] We did not find meta-analyses of tumor delineation in other solid cancers.

The variation in diagnostic performance may be explained by the notoriously difficult diagnostic problem to delineate glioma cells which gradually infiltrate into brain tissue. Therefore, the concept to delineate a tumor by presence or absence of cancer cells, on which ROC analysis is based, may oversimplify gradual glioma infiltration. Nevertheless, treatment target volumes are required for patient care.

Several factors may contribute to the observed variation in diagnostic performance. First, the scan protocols have not been standardized for any of these sequences. For the diagnostic standard of MRI, for instance, variation exists in scanner equipment, quality assessment and control, acquisition protocols, image processing, quantification, and interpretation by radiologists. Second, histopathological examination may vary due to incomplete sampling of heterogeneous tumors, and due to interpretation differences between neuropathologists.[113-115] Third, the correlation between imaging measurements and histopathological examination may be another source of variation. This co-localization depends on the precision of the navigated locations of tissue samples. Navigation precision has been found to be within several millimeters,[116,117] whereas tissue may be heterogeneous at smaller distances.[118]

Improvement of diagnostic accuracy to delineate glioma for regional therapy requires an offset between increasing the true positive rate and decreasing the false positive rate. Increasing the true positive rate may be preferable for tumor control, whereas decreasing the false positive rate may be preferable for preservation of functional integrity. From the perspective of tumor control the overestimation of diffuse glioma, i.e. the inadvertent declaration of normal brain as diffuse glioma, would be more acceptable than underestimation. But this is only acceptable when at the same time surgery aims to minimize neurological deficits from removal of critical brain regions whether or not infiltrated by tumor. This is usually done by brain mapping of functions under local anesthesia to push the resection to the functional limits.[90] In other words, a more sensitive imaging delineation would even more so require functional brain mapping as

a safeguard against removal of critical brain regions, that are potentially infiltrated by tumor. In this perspective, MR-spectroscopy and PET-imaging might hold potential to increase the true positive rate of glioma delineation for surgical strategies. However, a more sensitive tumor delineation should probably not prompt larger high-dose radiation fields, because a similar safeguard against cognitive decline from radiation therapy is unavailable. Perhaps high-dose radiotherapy should rather focus on regions at high-risk for tumor progression, whereas lower dose could be acceptable on regions with low-risk for tumor progression.

Our observations may challenge current care standards. First, T2/FLAIR-weighted MRI has been proposed as the standard for radiological response measurements in low-grade glioma,[88] whereas our data indicates T2-weighted MRI to have better diagnostic performance before treatment than T2/FLAIR-weighted MRI. Second, MRI, including T1-weighted gadolinium-enhanced and T2-weighted images, is considered the standard for treatment planning and radiological response measurements in high-grade glioma,[89] whereas our data indicates that the diagnostic performance of CT with contrast to delineate high-grade glioma before treatment is not necessarily inferior. Clearly, anatomy is better visualized with MRI than CT, another prerequisite to regional treatment planning. Furthermore, the detection of subtle areas of disease progression which may be outside the main tumor mass are better identified on MRI than on CT. Third, in particular for high-grade glioma there is room for improvement in tumor delineation. For instance, radiation oncology guidelines are heterogeneous with regards to target delineation.[44,119,120] MR spectroscopy and PET hold promise to be additive to the current standard, but availability and standardization are limitations to more widespread use. For a detailed discussion of these techniques we refer to recent reviews.[84,121-124] Furthermore, T2-weighted MRI performed best for diffuse gliomas as a whole and for low-grade-glioma, but could not be estimated for high-grade glioma in this data because quantitative information was only available from two studies. Nevertheless, T2-weighted MRI may contribute to better delineation of high-grade glioma as well.

Strengths of this meta-analysis include a scrutinous search strategy, assessment of reporting quality by STARD criteria, and analysis using the hsROC method, whenever available with individual sample data.

Our results should be interpreted within the limits of the quality of observational data that were retrieved with limited numbers of patients and samples from publications

with suboptimal reporting quality. Due to obvious reluctance to sample tissue outside of imaging abnormalities, true negative samples are underrepresented in this data, rendering the estimates of false positive rates probably less reliable than true positive rates. Furthermore, the available data only allowed indirect comparison of imaging techniques, because only two studies were identified with quantitative head-to-head comparison of techniques.[54,59] Lastly, several potential biases in this meta-analysis should be considered.[125] Methodological heterogeneity is likely to exist. Publication bias was suggested. Population bias is unlikely to be present, because all patients were required to have a glioma, control cases were excluded, and all samples from patients were examined with the same reference standard of histopathological examination. Nevertheless, verification bias may be present, because imaging characteristics have probably guided biopsy sampling strategies. The studies may be biased by patient selection and we cannot exclude heterogeneity from subjective interpretation of image measurements. Furthermore, clinical heterogeneity is likely to exist, because in addition to unstandardized imaging and pathology protocols, positivity criteria of diagnostic and reference tests may have varied between studies.

The implication of our findings is that planning of surgery or radiotherapy for diffuse gliomas using current imaging protocols should be done with caution, because these have only moderate accuracy for glioma delineation based on limited evidence. The sensitivity of imaging to delineate all regions of existing tumor infiltration seems to be less than the specificity to rule out tumor from normal brain. The true positive rate of conventional imaging for high-grade glioma may be improved by MR-spectroscopy and PET-imaging. Furthermore, future efforts to quantify and improve this accuracy may aim at combinations of imaging and head-to-head comparison with molecular characterization as gold standard.

CONCLUSIONS

In this meta-analysis, the diagnostic accuracy of imaging for delineation of diffuse glioma (low- and high-grade glioma combined) is best using T2-weighted MRI, followed by MR spectroscopy. The diagnostic accuracy of the common clinically utilized imaging is better for low-grade glioma using T2-weighted MRI than for high-grade glioma using T1-weighted gadolinium-enhanced MRI. Improvement is indicated for high-grade glioma using advanced imaging techniques, such as MR-spectroscopy and PET. Current imaging

protocols are based on limited evidence from heterogeneous studies and future studies with head-to-head comparison and combinations of imaging techniques are required to improve glioma delineation.

Supplemental Methods 1 | Search strategy to identify publications in mesh and emtree terms

MESH subject heading search: "glioma"[mesh] AND ("Diagnostic Imaging"[mesh] OR "Magnetic Resonance Spectroscopy"[mesh]) AND ("Brain Neoplasms/pathology"[Mesh] OR "Brain/pathology"[Mesh])

EMTREE subject heading search: 'glioma' and ('positron emission tomography' or 'nuclear magnetic resonance imaging') and ('pathology' or 'histopathology')

Supplemental Methods 2 | Example Bayesian code (jags) for hierarchical summary ROC model

```
### EXAMPLE DATA

# STUDY 1 as use case for 2x2 aggregated study data
# STUDY 2 as use case for individual data with 7 ordinal categories/levels
# N1/2 : number of observations
# ncat1/2 : number of test categories/levels
# Y1/2 : test category level for each observation [1 to ncat]
# D1/2 : disease status for each observation [0=non-diseased; 1=diseased]

N1=15,
ncat1=2,
Y1=c(1, 1, 2, 2, 2, 2, 2, 2, 2, 2, 2, 2, 2, 2, 2),
D1=c(0, 0, 1, 0, 1, 1, 1, 1, 1, 1, 1, 0, 1, 1, 1),
N2=52,
ncat2=7,
Y2=c(1, 2, 2, 2, 2, 2, 3, 3, 3, 3, 3, 3, 3, 4, 4, 4, 4, 4, 4, 4, 4, 4, 4, 4, 4, 4, 4, 4, 4, 4, 4, 5, 5,
5, 5, 5, 5, 5, 5, 5, 5, 5, 5, 5, 6, 6, 6, 6, 6, 6, 7),
D2=c(1, 0, 0, 0, 1, 1, 0, 1, 1, 1, 1, 1, 1, 1, 0, 0, 0, 0, 0, 0, 0, 0, 1, 1, 1, 1, 1, 1, 1, 1, 1, 1, 0, 0,
0, 0, 0, 0, 0, 0, 0, 0, 0, 1, 1, 0, 0, 0, 1, 1, 1, 1),

### PRIORS

# example for one neuro-imaging modality, here CT
# b_ : beta (scale parameter)
```

```
# a_ : alpha (accuracy parameter)
# ta_ : precision of the accuracy parameter (tau of alpha)
# t_ : theta (cutpoint parameter)
# tt_ : precision of the cut point parameter (tau of theta)

b_CT ~ dnorm(0.0,1.0E-4)T(-10,10)
a_CT ~ dnorm(0.0,1.0E-4)
ta_CT ~ dgamma(0.01,0.01)
t_CT ~ dnorm(0.0,1.0E-4)
tt_CT ~ dgamma(0.01,0.01)

### SUMMARY ESTIMATES

# stpr_ : summary true positive rate
# sfpr_ : summary false positive rate
# dor_ : summary diagnostic odds ratio
# auc_ : summary area under the ROC curve

stpr_CT <- 1 / (1 + exp(-( (t_CT + a_CT/2) * exp(-b_CT/2) )) )
sfpr_CT <- 1 / (1 + exp(-( (t_CT - a_CT/2) * exp( b_CT/2) )) )
dor_CT <- ( stpr * (1 - sfpr) ) / ( (1 - stpr) * sfpr )

for (i in 1:100) { tfpr[i] <- (i - 1) * 0.01 }
for (i in 1:100) { ttpr_CT[i] <- 1 / (1 + exp(-(a_CT * exp(-b_CT/2) + exp(-b_CT) * log(tfpr[i]/
(1-tfpr[i])) ))) }
ttpr_CT[101] <- 1
auc_CT <- 0.01*(ttpr_CT[1]/2 + sum(ttpr_CT[2:100]) + ttpr_CT[101]/2)

### MODEL

#---Study 1--- example of aggregated 2x2 study data

# model the cumulative probabilities (Q)
for (i in 1:N1) {
  Q1[i] <- 1 / (1 + exp(-( (theta1 - alpha1 * (D1[i]-0.5)) * exp(-beta1 * (D1[i]-0.5)) )))
  # Create P from cumulative P (i.e., Q)
```

```
  P1[i, 1] <- min(max(Q1[i], 0), 1)
  P1[i, ncat1] <- min(max(1-Q1[i], 0), 1)
  # Discretize P to create Y
  Y1[i] ~ dcat(P1[i, 1: ncat1])
  }

# Distribution for alpha1 (accuracy) and beta1 (scale) and theta1 (cutpoint/positivity)
beta1 <- b_CT
alpha1 ~ dnorm(a_CT,ta_CT)
theta1 ~ dnorm(t_CT,tt_CT)

#---Study 2--- example of multilevel individual data

# model the cumulative probabilities (Q)
for (i in 1:N2) {
  for (j in 1:(ncat2-1)) { Q2[i,j] <- 1 / (1 + exp(-( (theta2[j] - alpha2 * (D2[i]-0.5)) * exp(-
  beta2 * (D2[i]-0.5)) ))) }
  # Create P from cumulative P (i.e., Q)
  P2[i,1] <- min(max(Q2[i,1], 0), 1)
  for (r in 2:(ncat2-1)) { P2[i, r] <- Q2[i,r] - Q2[i,(r-1)] }
  P2[i, ncat2] <- min(max(1-Q2[i, ncat2-1], 0), 1)
  # Discretize P to create Y
  Y2[i] ~ dcat(P2[i, 1: ncat2])
  }

# Distribution for alpha2 (accuracy) and beta2 (scale) and theta2 (cutpoint/positivity)
beta2 <- b_CT
alpha2 ~ dnorm(a_CT,ta_CT)
for(t in 1:6) {theta2_0[t] ~ dnorm(t_CT,tt_CT)}
theta2[1:6] <- sort(theta2_0)
```

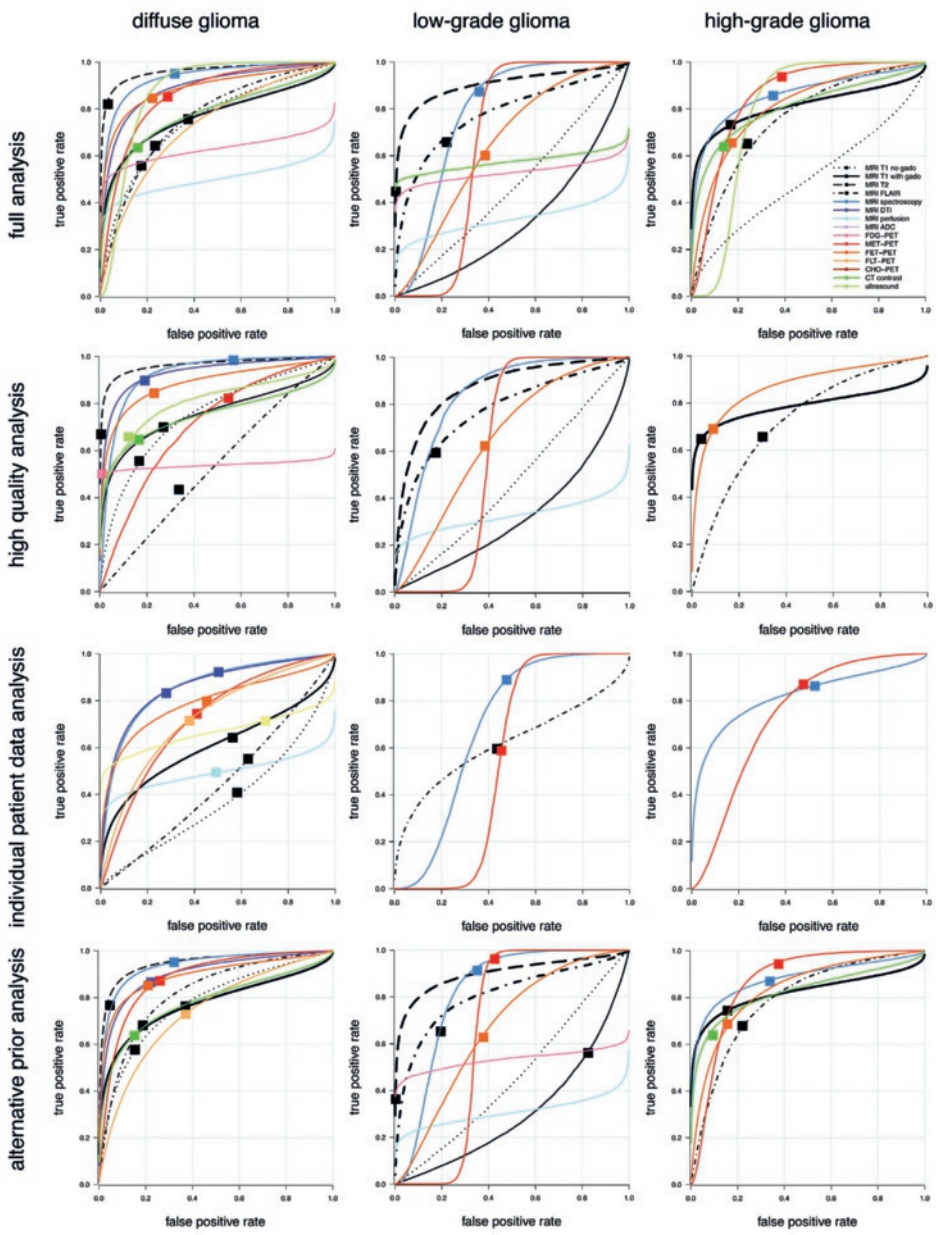

Supplemental Figure 1 | Sensitivity analysis with results from subset of high-quality studies, individual patient data studies, and alternative vague priors.

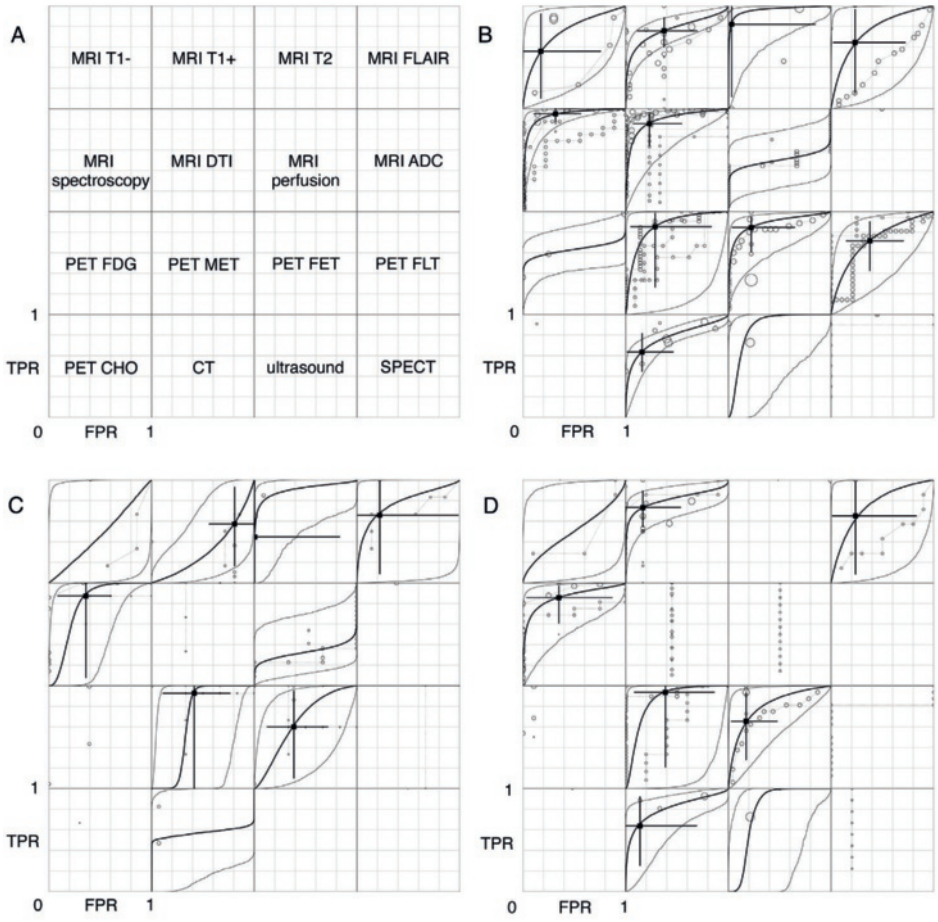

Supplemental Figure 2 | Summary hierarchical ROC curves of imaging techniques with individual study data. A) legend of imaging techniques, B) diffuse glioma studies, C) low-grade glioma studies, D) high-grade glioma studies. Envelopes of 95%CIs for hsROC curves are plotted in thinner lines. Operating points for summary false positive and summary true positive rates are shown with 95%CIs. The size of circles corresponds with study sample size. Circles connected by lines represent a ROC curve for individual studies based on individual patient data.

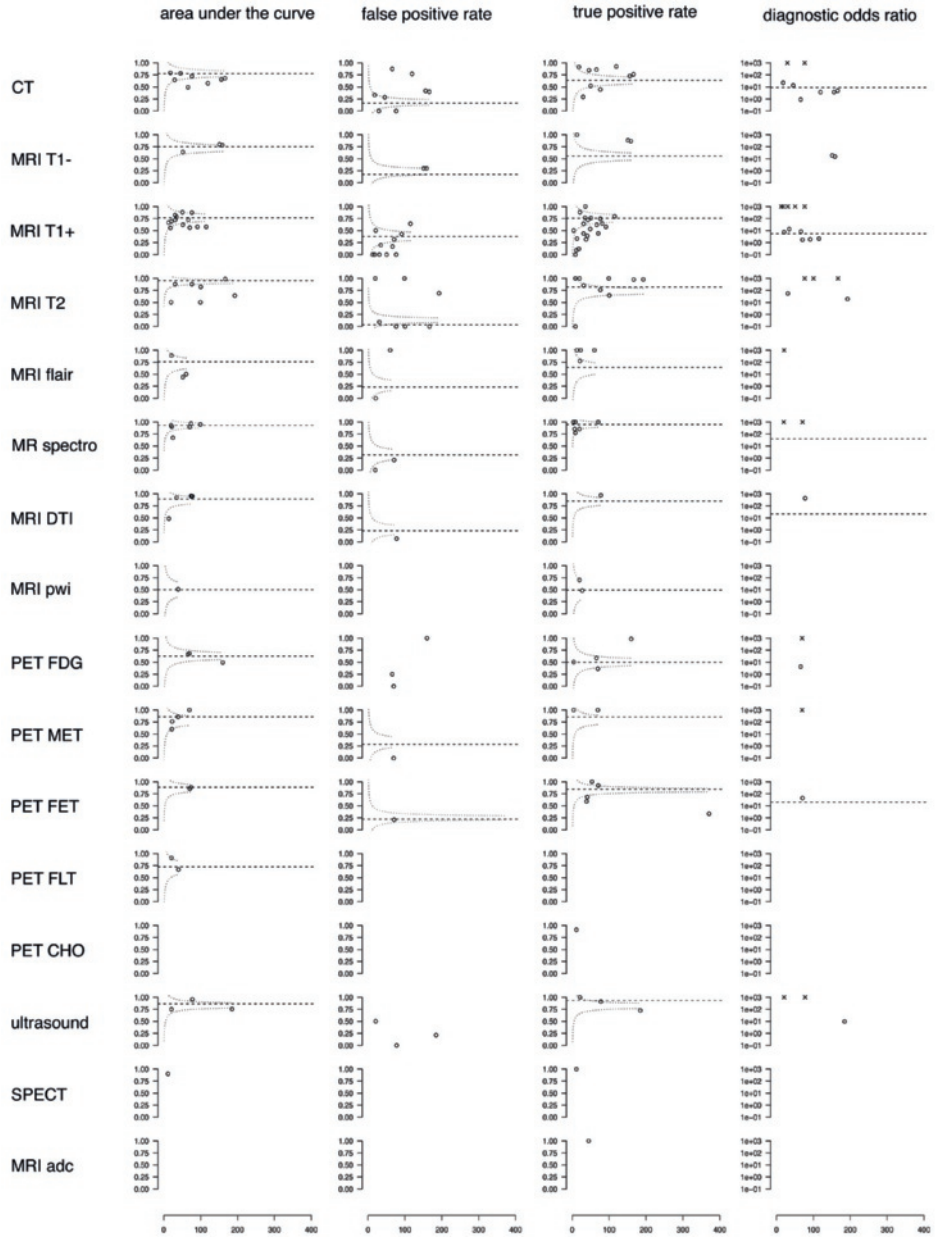
area under the curve
false positive rate
true positive rate
diagnostic odds ratio
CT
MRI T1-
MRI T1+
MRI T2
MRI flair
MR spectro
MRI DTI
MRI pwi
PET FDG
PET MET
PET FET
PET FLT
PET CHO
ultrasound
SPECT
MRI adc

Supplemental Figure 3 | Exploration of publication bias plotted by sample size versus outcome measures (area under the curve, false positive rate, true positive rate, and diagnostic odds ratio) per imaging technique. Points correspond with individual studies. Crosses indicate diagnostic odds ratios, truncated at 1,000. Horizontal dotted lines represent summary estimates of outcome measures. Most imaging modalities have insufficient numbers of studies to evaluate publication bias, but there is an indication that small studies with small areas under the curve or low false positive rates may be missing for T1-weighted gadolinium-enhanced MRI and T2-weighted MRI.

Supplementary Table 1 | PRISMA Checklist

Section/topic	#	Checklist item	Page
TITLE			
Title	1	Identify the report as a systematic review, meta-analysis, or both.	Title page
ABSTRACT			
Structured summary	2	Provide a structured summary including, as applicable: background; objectives; data sources; study eligibility criteria, participants, and interventions; study appraisal and synthesis methods; results; limitations; conclusions and implications of key findings; systematic review registration number.	p.1/2
INTRODUCTION			
Rationale	3	Describe the rationale for the review in the context of what is already known.	p.4/5
Objectives	4	Provide an explicit statement of questions being addressed with reference to participants, interventions, comparisons, outcomes, and study design (PICOS).	p.5
METHODS			
Protocol and registration	5	Indicate if a review protocol exists, if and where it can be accessed (e.g., Web address), and, if available, provide registration information including registration number.	NA
Eligibility criteria	6	Specify study characteristics (e.g., PICOS, length of follow-up) and report characteristics (e.g., years considered, language, publication status) used as criteria for eligibility, giving rationale.	p.6/7
Information sources	7	Describe all information sources (e.g., databases with dates of coverage, contact with study authors to identify additional studies) in the search and date last searched.	p.5

Section/topic	#	Checklist item	Page
Search	8	Present full electronic search strategy for at least one database, including any limits used, such that it could be repeated.	Supp methods 1
Study selection	9	State the process for selecting studies (i.e., screening, eligibility, included in systematic review, and, if applicable, included in the meta-analysis).	p.6
Data collection process	10	Describe method of data extraction from reports (e.g., piloted forms, independently, in duplicate) and any processes for obtaining and confirming data from investigators.	p.6/7
Data items	11	List and define all variables for which data were sought (e.g., PICOS, funding sources) and any assumptions and simplifications made.	p.6/7
Risk of bias in individual studies	12	Describe methods used for assessing risk of bias of individual studies (including specification of whether this was done at the study or outcome level), and how this information is to be used in any data synthesis.	p.9
Summary measures	13	State the principal summary measures (e.g., risk ratio, difference in means).	p.8/9
Synthesis of results	14	Describe the methods of handling data and combining results of studies, if done, including measures of consistency (e.g., I^2) for each meta-analysis.	p.8/9
Risk of bias across studies	15	Specify any assessment of risk of bias that may affect the cumulative evidence (e.g., publication bias, selective reporting within studies).	p.9
Additional analyses	16	Describe methods of additional analyses (e.g., sensitivity or subgroup analyses, meta-regression), if done, indicating which were pre-specified.	p.9
RESULTS			
Study selection	17	Give numbers of studies screened, assessed for eligibility, and included in the review, with reasons for exclusions at each stage, ideally with a flow diagram.	p.9 & fig.1
Study characteristics	18	For each study, present characteristics for which data were extracted (e.g., study size, PICOS, follow-up period) and provide the citations.	p.9/10, fig 2 & Supp Data
Risk of bias within studies	19	Present data on risk of bias of each study and, if available, any outcome level assessment (see item 12).	p.10 & Supp Data
Results of individual studies	20	For all outcomes considered (benefits or harms), present, for each study: (a) simple summary data for each intervention group (b) effect estimates and confidence intervals, ideally with a forest plot.	Supp Data

Section/topic	#	Checklist item	Page
Synthesis of results	21	Present results of each meta-analysis done, including confidence intervals and measures of consistency.	p.11/12, fig 3 & fig 4
Risk of bias across studies	22	Present results of any assessment of risk of bias across studies (see Item 15).	p.12 & Supp fig 2 & 3
Additional analysis	23	Give results of additional analyses, if done (e.g., sensitivity or subgroup analyses, meta-regression [see Item 16]).	p.12 & Supp fig 1
DISCUSSION			
Summary of evidence	24	Summarize the main findings including the strength of evidence for each main outcome; consider their relevance to key groups (e.g., healthcare providers, users, and policy makers).	p.13
Limitations	25	Discuss limitations at study and outcome level (e.g., risk of bias), and at review-level (e.g., incomplete retrieval of identified research, reporting bias).	p.16/17
Conclusions	26	Provide a general interpretation of the results in the context of other evidence, and implications for future research.	p.17
FUNDING			
Funding	27	Describe sources of funding for the systematic review and other support (e.g., supply of data); role of funders for the systematic review.	Title page

From: Moher D, Liberati A, Tetzlaff J, Altman DG, The PRISMA Group (2009). Preferred Reporting Items for Systematic Reviews and Meta-Analyses: The PRISMA Statement. PLoS Med 6(6): e1000097. doi:10.1371/journal.pmed1000097

Niels Verburg
Philip C. de Witt Hamer

Submitted

Chapter 3

State-of-the-art imaging for glioma surgery

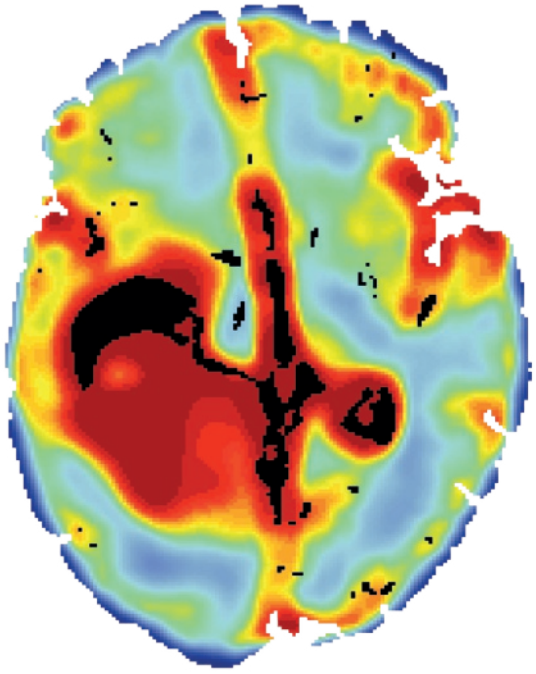

ABSTRACT

Diffuse gliomas are infiltrative primary brain tumors with a poor prognosis despite multimodal treatment. Maximum safe resection is recommended whenever feasible. The extent of resection (EOR) is positively correlated with survival. Identification of glioma tissue during surgery is difficult due to its diffuse nature. Therefore, glioma resection is imaging-guided, making the choice for imaging technique an important aspect of glioma surgery. The current standard for resection guidance in non-enhancing gliomas is T2 weighted or T2w- fluid attenuation inversion recovery magnetic resonance imaging (MRI), and in enhancing gliomas T1 weighted MRI with a gadolinium-based contrast agent. Other MRI sequences, like magnetic resonance spectroscopy, imaging modalities, such as positron emission tomography, as well as intraoperative imaging techniques are also available for the guidance of glioma resection. The neurosurgeon's goal is to find the balance between maximizing the EOR and preserving brain functions since surgery induced neurological deficits result in lower quality of life and shortened survival. This requires localization of important brain functions and white matter tracts to aid the pre-operative planning and surgical decision-making. Visualization of brain functions and white matter tracts is possible with functional MRI, diffusion tensor imaging, magnetoencephalography and navigated transcranial magnetic stimulation. In this review we discuss the current available imaging techniques for the guidance of glioma resection and the localization of brain functions and white matter tracts.

INTRODUCTION

Surgical resection is the first treatment in the majority of patients with a diffuse glioma. Surgery aims at providing adequate tissue for diagnosis, relieving mass effect and achieving cytoreduction. To achieve maximal cytoreduction, pursued to improve patient's survival,[8,43] the neurosurgeon needs to identify glioma infiltration during surgery. This is difficult due to the diffuse dissemination of glioma cells in the normal brain. The most widely used aid for the detection of glioma infiltration during surgery is imaging. Standard magnetic resonance imaging (MRI), T1-weighted gadolinium-enhanced (T1G) for enhancing gliomas (Figure 1A) and T2 (T2w) or fluid attenuation inversion recovery (FLAIR) weighted for non-enhancing gliomas (Figure 1B), is recommended.[38]

These standard MRI sequences, however, are less accurate for the detection of glioma infiltration than advanced MRI sequences and imaging modalities.[126] Therefore, advanced imaging holds the potential to expand the resection beyond the standard MRI abnormalities, which may improve patient's outcome.[7,127-130]

When expanding the resection, one must be aware of the potential loss of brain function due to the infiltration of tumor cells in normal functioning brain. Important brain functions, such as motor function, language, and neurocognitive functioning, need to be preserved since severe morbidity is not only associated with a decline in quality of life but also with survival.[131] The current standard to identify brain functions and white-matter tracts is intraoperative direct cortical stimulation (DCS), a technique that provides an electrical stimulation to accomplish local excitation or inhibition in the cortex or white matter tracts that will result in a functional response.[90] Multiple techniques are available for the localization of brain functions or white-matter tracts.

The neurosurgeon's goal is to find the balance between the optimal oncological outcome by maximizing the resection and preventing severe morbidity by loss of brain functionality. Here we discuss the state-of-the-art imaging techniques to guide glioma resection and imaging techniques to localize functions and white matter tracts, in order to achieve a maximal safe resection.

IMAGING TECHNIQUES FOR THE GUIDANCE OF GLIOMA RESECTION

Pre-operative imaging

***Standard MRI*.** The current standard MRI sequences for the guidance of glioma resection have historically grown into use since their widespread availability. Clinical trials supporting the use of standard MRI for the guidance of glioma resection are lacking. Therefore, we discuss the indirect evidence for these sequences. This evidence comes from studies that investigated the effect of the extent of image-guided glioma resection on survival.

In enhancing glioma, the strongest evidence for the use of T1G MRI comes from a post-hoc analysis of 243 patients from a randomized controlled trial (RCT), comparing fluorescence-guided surgery with standard neuronavigation.[50,94] In this study – after correction for tumor size, edema, midline shift, location, age, Karnofsky Performance Scale and National Institutes of Health Stroke Scale – complete resection of contrast enhancement on post-operative T1G MRI, compared to incomplete resection, resulted in longer OS (16.7 versus 11.8 months, $p<0.01$).[94]

In non-enhancing glioma, the choice for T2w or FLAIR MRI aided surgery depends on the surgeon's preference, since direct comparison is lacking, which is reflected in the used imaging sequences in a recent review,[132] where T2w, FLAIR and T2w or FLAIR MRI were respectively used in 36%, 46% and 18% of the studies. A possible benefit of FLAIR MRI is the suppression of the water signal intensity, which allows for better contrast of tumor in periventricular areas. Both T2w and FLAIR MRI aided resections are supported by retrospective studies.[8,133] These studies prove the goal of complete resection of the standard MRI abnormalities in both enhancing and non-enhancing gliomas. The lack of studies directly comparing standard MRI- versus other imaging-guided resection, however, makes it impossible to judge if standard MRI is the best option for the guidance of glioma resection. Considering the evidence of diagnostic accuracy studies,[126] more is to be expected from other MRI sequences or imaging modalities.

FLAIR MRI in enhancing glioma. In the majority of enhancing glioma, FLAIR abnormalities expand beyond the regions with contrast enhancement (Figure 1A).[134] These surrounding FLAIR abnormalities are sometimes addressed as peritumoral edema, however, many studies have proven the presence of glioma cells within these regions.[3,53,64,66,135] Extending

the resection beyond contrast-enhanced regions using FLAIR has shown great potential. A large (n=643) retrospective study found an improved OS for a more extensive (≥53%) resection of the surrounding FLAIR abnormalities after complete resection of contrast-enhanced regions, compared to less extensive resections (median OS 20.7 and 15.5 months, respectively; p<0.01). Remarkably, a more extensive resection resulted in a lower complication rate (18% versus 26%, p=0.04), which reflects, according to the authors, the increased use of DCS and imaging to visualize brain functions and white matter tracts. These promising results are a bit tempered by the fact that an extensive resection was only achieved in 25% of the patients.[7] Both FLAIR resection threshold, number of patients receiving extensive resection and the lower complication rate with more extensive resection were confirmed in another study with 282 patients.[128] These are the largest studies comparing, although not randomized and prospective, different MRI sequences to aid glioma resection, therefore providing the strongest evidence for the use of other sequences than the current standard.

Magnetic Resonance Spectroscopy Imaging. Magnetic Resonance Spectroscopy Imaging (MRSI) measures biochemical components of a region of interest, which can be used to calculate, among others, the choline-N-acetyl aspartate index (CNI) to detect glioma (Figure 1A and B). The only study describing MRS aided surgery reported an extended resection beyond contrast enhancement in 86% of seven enhancing gliomas and beyond FLAIR MRI abnormalities in 88% of eight non-enhancing gliomas. The target volume for resection was based on the lowest CNI threshold that allowed a safe resection, defined by functional imaging and anatomy. The survival benefit in this study is not clear due to the limited follow-up of one year, in which one enhancing glioma and none of the non-enhancing gliomas recurred.[79] A limitation of MRSI is the technical difficulty of obtaining a good quality 3D MRS image due to the artifacts of non-brain tissue.[136] The concept of different threshold based target volumes, as well as the possibility to aid resections beyond FLAIR abnormalities, makes MRSI an interesting technique that deserves further research.

Positron emission tomography. Positron emission tomography (PET) is a nuclear imaging technique that uses radioactive tracers to visualize perfusion, proliferation, metabolism and neurotransmitters (Figure 1A and B). Multiple tracers are available for glioma imaging of which only the amino acid L-[methyl-11C]methionine (MET) is used to aid glioma resection. The only group reporting MET PET aided resection selected gliomas with ill-defined borders or enhancing gliomas with T2w or FLAIR abnormalities beyond

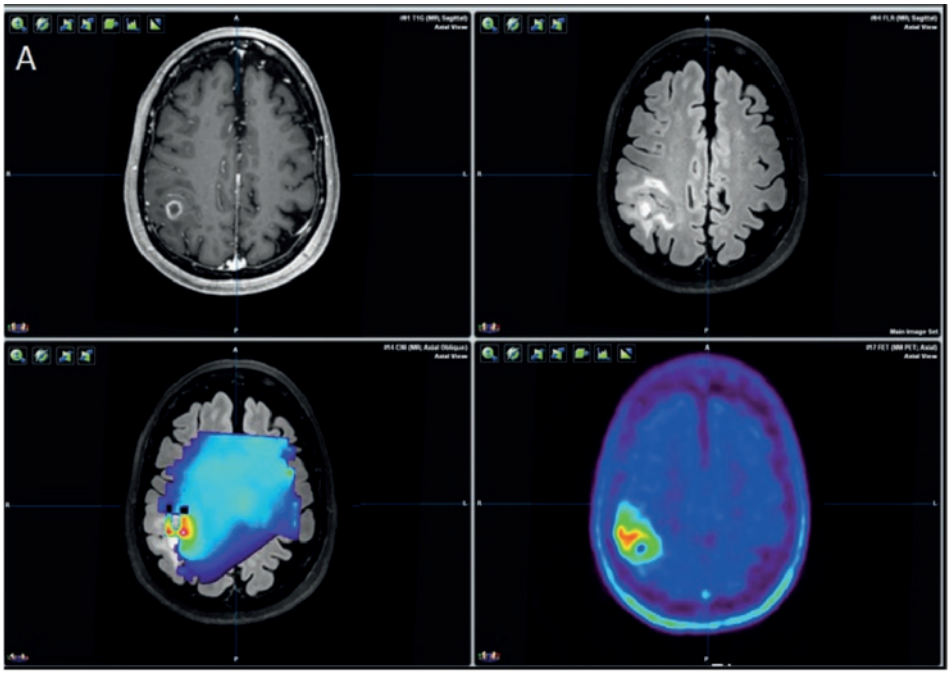
A

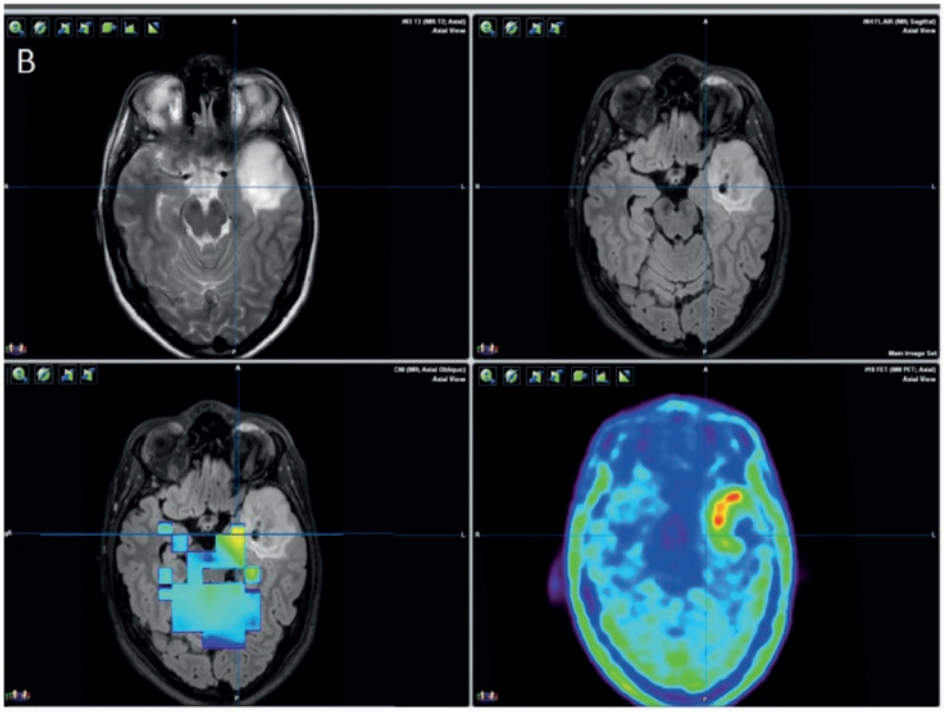
B

Figure 1 | Exemplary standard and advanced imaging

A) Patient with a right parietal enhancing glioblastoma, IDH-wildtype. *Upper left*: T1 weighted MRI with a gadolinium-based contrast agent, *Upper right*: FLAIR MRI, Lower left: multivoxel MRSI CNI projected on the FLAIR MRI. *Lower right*: amino acid ([^{18}F]FET) PET. B) Patient with a left temporal non-enhancing diffuse astrocytoma, IDH-mutant. The crosshair is projected to indicate the region with MRSI CNI and PET abnormalities just outside the FLAIR MRI abnormalities. *Upper left*: T2 weighted MRI, *Upper right*: FLAIR MRI, *Lower left*: multivoxel MRSI CNI projected on the FLAIR MRI, *Lower right*: amino acid ([^{18}F]FET) PET.

the contrast enhancement. Two strategies were used for these gliomas: 1) to extent the resection beyond standard MRI abnormalities or 2) a focused resection of the most metabolic active parts of the tumor if a complete resection of MRI abnormalities was not possible. In enhancing gliomas, each strategy was achieved in one-third of patients, while PET was not contributive in the remaining one-third of patients. In non-enhancing gliomas, the first strategy was achieved in 74%, the second strategy in 14% and 12% of patients did not have a contributive MET PET. OS in enhancing gliomas was predicted by complete resection of MET uptake, achieved in 56% of patients, while complete resection of contrast-enhancement, achieved in 35% of patients, did not.[129] Unfortunately, survival data was not collected. Limitations of PET imaging are the costs, estimated 1600–2100 dollar for one scan,[137] although a cost-effectiveness analysis showed that use of MRI and PET is cost-effective.[138] Other limitations are the necessity of an on-site cyclotron for tracers with a short half time and one-third of the non-enhancing gliomas are amino acid PET negative.[139] Although these retrospective results are biased by the specific inclusion criteria and the low percentage of complete resection of contrast enhancement, they show the potential of PET aided glioma surgery.

***Limitations pre-operative imaging*.** Three limitations of all pre-operative imaging are interobserver variation for tumor delineation, image fusion and registration setup inaccuracy, and inability to compensate for intraoperative surgery induced changes. Interobserver variation for the delineation of gliomas is the difference in tumor volumes, as assessed on imaging, between different interpreters. In enhancing gliomas, this in only a minor issue since observer agreements are good (range 0.97–0.99).[140,141] In non-enhancing gliomas, however, agreements are considerable lower (range 0.48–0.77) for both T2w and FLAIR MRI.[141,142] Possible causes for this lower agreement are the interpretation of the hyperintense T2w and FLAIR signal as edema or glioma infiltration and the less well-defined borders of the T2w and FLAIR abnormalities.[141] MRSI and PET

are less limited by inter-observer variability due to their quantitative analysis and the use of a threshold. Image fusion and registration setup inaccuracy occurs due to the translation of post-operative images to the intra-operative situation. Since the intra-operative navigation is based on the 3D model of one MRI sequence, mostly 3D T1G or 3D FLAIR MRI, all other images that are used for the delineation need to be fused with this 3D sequence. This fusion is mostly performed with a linear method and inaccuracies of 1.0 to 3.0 mm have been reported.[143] Registration inaccuracy occurs due to the translation of the 3D MRI model to the actual patient. Depending on setup, inaccuracy varies between 1.59 and 3.86 mm.[144] The last but foremost limitation is the inability of pre-operative imaging to adjust to the new situation after surgical induces changes such as brain shift, tissue deformation and tissue removal. Shifts between 7mm inward and 8mm outward were found after dura opening, and 9.7mm inward and 15mm outward (mean 2.7–5.4mm) after tumor resection.[145,146] The influence of these effects on the resection can be limited by circumscribing the tumor, instead of piecemeal removal, thereby limiting the brain shift.

Intra-operative imaging

Intra-operative MRI. Intra-operative MRI (iMRI) has the advantage over pre-operative MRI that it can overcome its above-mentioned limitations. Since the images are acquired in the same position as the surgery, registration inaccuracy is lower for iMRI than pre-operative MRI.[147] Even more important, iMRI can visualize the altered anatomy due to intra-operative changes, which reduces their influence on navigation inaccuracy (Figure 2A).[148]

Besides these advantages in navigation accuracy, iMRI allows for the detection of residual tumor after a first attempt for a maximal resection. In enhancing glioma, a RCT with 49 patients found a higher percentage of complete resections of contrast enhancement in the iMRI group (96% versus 68%, $p<0.01$),[149] although the effect on survival is still awaited for. In non-enhancing glioma, multiple retrospective studies report improved complete resection rates (14 to 19%) of T2w or FLAIR abnormalities using iMRI.[150-152] Two major drawbacks of iMRI are the high initial costs, 3.8 million dollar for the ultra low-field model in 2011 and the prolonged duration of the surgery, up to 2 hours, due to scan time.[153,154] Although iMRI has proven its value for the purpose of complete resection of standard MRI abnormalities, studies using iMRI to extend the resection beyond these standard imaging abnormalities are lacking. Even if this is possible, alternatives could be considered due to the high cost and prolonged surgical time of iMRI.

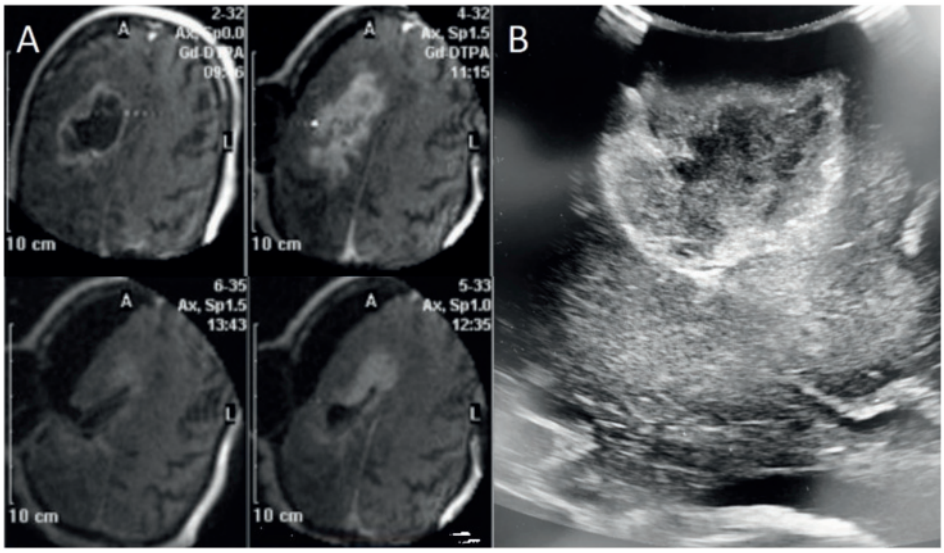

Figure 2 | Examples of intra-operative imaging.

A) Intra-operative MRI of an enhancing right frontal glioblastoma with clockwise images of the progression of the resection with clear brain shift. Image courtesy of dr. P Kubben.[155] B) Intra-operative ultrasound of a left parietal glioblastoma.

Ultrasound. The visualization of returning sound waves can be used to detect glioma by direct application of the ultrasound (US) probe on the tissue (Figure 2B). Like with iMRI, this results in real-time imaging that is not influenced by navigation inaccuracy or intra-operative changes. US guided resection achieved a complete resection of US abnormalities in 67% of the 61 enhancing and 61% of the 51 non-enhancing glioma patients. This resulted in an improved two-year OS compared to a random selected control group (32.8% versus 13.3% and 88.2% versus 53.3%, both $p<0.05$, respectively enhancing and non-enhancing glioma).[156] New US techniques like high frequency linear probes and ultrasonic contrast are introduced and hold potential to maximize resections compared to standard US.[157,158] Direct comparison of high frequency US with iMRI, using biopsies from residual tumor and normal control sites after resection, resulted in a significant higher sensitivity for US (sensitivity 76% versus 55%, $p=0.021$) and not significant difference in specificity (specificity 74% versus 58%).[159] Besides detection of glioma tissue, US can be used to update the pre-operative MRI based neuronavigation.[160] Limitations of US are the training necessary to create a good quality image; problems with artifacts due to blood, hemostatic material, bone and other structures material;

and the 2D aspect of US. This makes the acquisition and interpretation of US for glioma delineation challenging.[81] Still, US can serve as a good and cheaper alternative for iMRI.

IMAGING FOR LOCALIZATION OF BRAIN FUNCTIONS AND WHITE-MATTER TRACTS

Pre-operative imaging

Functional MRI. BOLD-Functional MRI (fMRI) measures the blood oxygenation level changes caused by perfusion, which is a surrogate for neuronal activity. This allows for visualization of specific tasks-related activity such as motor function or language (Figure 3A).[161] Applying fMRI to localize language areas resulted in a 59–100% sensitivity and 0-97% specificity in a systematic review, with the wide ranges attributed to the heterogeneity in language tasks and imaging protocols. The authors conclude that fMRI is not an alternative for DCS language mapping.[162] Accuracy for motor function localization, compared to DCS, varies between studies, with smaller studies reporting higher accuracies (up to 100%) than the larger studies (66–72%).[163-166] In the largest study, 210 cortical sites were tested in 29 patients, resulting in a 83% sensitivity and 82% specificity. In patients with glioblastoma, however, sensitivity was only 65%, which is, according to the authors, a possible effect of the neurovascular uncoupling.[167] The limitations of fMRI have been recently described extensively and include: statistical power, flexibility in data-analysis, multiple comparisons, software errors, insufficient study reporting and lack of independent replications.[168,169] Taken together, fMRI is not accurate enough to aid in the surgical planning, let alone replace DCS.

Diffusion Tensor Imaging. Diffusion Tensor Imaging (DTI) is a technique that relies on Brownian movement of water molecules in tissue. The direction of these movements is restrained in white matter fibers, which can be used to visualize the anatomical location of white matter tracts, so-called DTI tractography (Figure 3B).[170] This technique solemnly visualizes anatomy and does localize brain functionality. Studies comparing DTI tractography with the gold standard DCS reported mean distances between DTI tractography and positive stimulations of 5.2 to 8.7mm.[77,171,172] Therefore a minimum safe distance of 10mm from a tract has been recommended. In a RCT comparing resection with and without pre-operative DTI in 214 patients with diffuse glioma involving the pyramidal tract, the use of DTI in patients with enhancing glioma resulted in a higher complete resection rate (74.4% versus 33.3%, $p<0.001$), 6-months good

clinical condition (70.0% versus 36.8%, p=0.001) and improved OS (0.570, 95%CI, 0.325–1.003; p=0.05). In non-enhancing glioma patients, complete resection rate did not significantly differ, yet 6-months good clinical condition was higher in the DTI group (93.4% versus 79.1%, p=0.013).[173] Although this study clearly shows the benefit of DTI tractography in glioma resection, one must take into account that 63% of patients in the control group had a poor clinical condition 6-months after surgery, which is remarkably high and would exclude these patients from adjuvant therapy in most neuro-oncology centers. High angular resolution diffusion-weighted imaging (HARDI) with q-ball algorithms is a new tractography technique with improved fiber tracking resolution at voxels with crossing fiber populations.[174,175] One study reported that an intact left arcuate fasciculus and temporal part of the superior longitudinal fasciculus on post-operative HARDI tractography was associated with intact language, whereas an alteration or damaging of these structures resulted in respectively, temporary or long-term language deficits.[176] Limitations of DTI are the variability of tracking algorithm settings and region-of-interest (ROI) placement. Tracking algorithm settings can lead to under-, but mostly overestimation of white-matter tracts. Still, 90% of the ground truth fibers are present in most of the algorithms.[177] ROI placement is subject to moderate to substantial interobserver variability, but can be improved with protocols for ROI positioning.[178] Also, for HARDI DTI considerable technical expertise is required, making it not yet available for standard practice. The high sensitivity and proven clinical value make DTI an indispensable technique for glioma surgery.

Magnetoencephalography. Magnetoencephalography (MEG) detects magnetic fields as result of the electric currents from neuronal activity.[179] Although this is not an imaging technique, registration of the MEG with a 3D MRI sequence allows for visualization (Figure 3C). Like fMRI, MEG can be used for the assessment of task-based activity in the pre-operative phase. Two small studies found MEG predicted motor function areas at 4 to 17mm from DCS sites.[180,181] A direct comparison of MEG en fMRI for the localization of the motor cortex showed an overlap with DCS in, respectively, 100% and 73% of the patients,[182] demonstrating the higher accuracy of MEG. Indirect evidence shows that MEG predicted functional areas within or at the margin the tumor resulted in a partial resection in 88% and complete resection in 12%, with neurological deterioration in 36% and 100%, respectively.[183] On the other hand, using sensorimotor, visual and speech MEG as a risk assessment for operation feasibility resulted in 46% of patients not to be considered for surgery due to glioma invasion of functional cortex, with only 6% of the patients who were operated suffering from neurological deterioration.[184] A major

limitation of MEG is the availability, mostly in dedicated academic centers, and technical expertise needed to interpret the results. Therefore, although accuracy is considerable and clinical application proven, MEG is not likely to become a standard modality in glioma treatment.

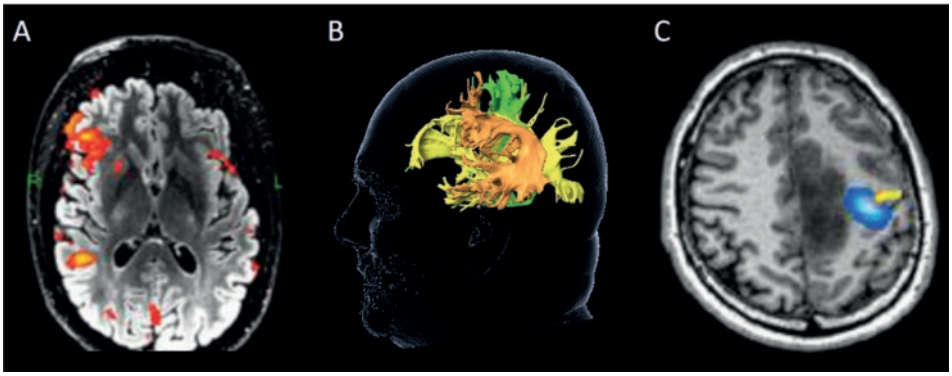

Figure 3 | Examples of imaging for localization of brain functions and white-matter tracts.

A) Functional MRI of a patient with a language located in the right hemisphere, which was confirmed with a WADA test. B) Visualization of the left corticospinal tract (green), fasciculate arcuatus (orange) and inferior fronto-occipital fasciculus (yellow) using DTI in a patient with a left temporal diffuse astrocytoma, IDH-mutant. C) Localization of the left motor cortex using MEG in a patient with a diffuse astrocytoma, IDH-mutant.

Transcranial Magnetic Stimulation. Transcranial Magnetic Stimulation (TMS), like MEG, is not an imaging technique. Due to the integration with neuronavigation (nTMS), however, it can be used to locate and visualize brain functions in the pre-operative phase. By stimulating or inhibiting cortical activity with directed magnetic fields, specific functional tasks can be localized.[185] The accuracy of nTMS, compared with DCS, for localization of the motor cortex is between 3.4–6.2 mm.[186,187] Another function of nTMS is the combination with DTI tractography, where nTMS regions, instead of user-selected regions of interest (ROI), are used to guide the tractography. In a study comparing ROI-based with nTMS-based tractography for language pathways, respectively, 40% and 76% of the tracts were detected with DSC.[188] Using nTMS for pre-operative planning, multiple studies found a minimum distance (range 8–12mm) from nTMS motor function or nTMS-fiber tracking that prevented any neurological deterioration.[188-190] Clinical implementation of nTMS in a large (n=250) cohort of patients with brain tumors in motor eloquent

locations, in comparison with a historical case-matched non-nTMS cohort, resulted a significantly increased complete resection rate (59% versus 42%, p=0.05; respectively) and increased PFS for patients with non-enhancing glioma (15.4 months versus 22.4 months, p=0.05; respectively). Planned biopsies or non-surgical strategies were changed into resections in 68.5% and overall postoperative deficit rate did not significantly differ between the groups (6.1% versus 8.5%; respectively). [191] One must realize that DCS was still used in 66% of the patients and that the authors conclude that nTMS is crucial for preoperative planning.

Only one small (n=4) study used nTMS and nTMS tractography instead of DCS in patients not suitable for awake surgery with left sided perisylvian lesions. This resulted in a GTR in all patients without any new neurological deficit with only one patient needing a second nTMS based resection within days to achieve the GTR.[192] Overall, nTMS is a promising new technique that, combined with DTI, can overcome the ROI selection limitation of DTI and has proven is usefulness for surgical planning.

Intra-operative imaging

Intra-operative MRI. Both fMRI and DTI can be acquired intra-operatively using iMRI. Intra-operative fMRI (ifMRI) can successfully localize the motor cortex during awake procedures using the task-based fMRI technique.[193] More interesting is the use of ifMRI resting-state that allows for the localization of the motor cortex in patients under general anesthesia.[194,195] Comparison of this technique with DCS in 14 patients resulted in a 62% sensitivity and 94% specificity.[195] Intra-operative DTI (iDTI) tractography has a high accuracy (100% sensitivity and 72% specificity) for the localization of the corticospinal tract, as demonstrated in a study with twenty glioma patients.[196] Another study replaced DCS with iDTI tractography for the localization of white-matter tracts involved in language, resulting in a GTR in 78% and PR in 22% of the patients without any postoperative neurological deterioration.[197] The limitations of iMRI have been described above. Although ifMRI is not likely to replace DCS, iDTI has the potential to increase the safety of non-awake surgery.

DISCUSSION

How can imaging aid glioma surgery? We know glioma are widespread in the brain by the time of diagnosis, so a curative resection is not possible.[198] Still, there is accumulating evidence that removing more of the tumor improves PFS and OS.[8,43] Since glioma is an infiltrative disease, macroscopic recognition of the tumor within the normal brain can be very difficult. Imaging has the possibility to visualize the tumor and thus overcoming the macroscopic problems. Ideally an imaging modality would not miss any tumor, 100% sensitivity, and only show tumor, 100% specificity.

Unfortunately current available imaging is not that accurate.[126] Still, using the current standard MRI to guide glioma resection has a positive impact on the treatment. Intraoperative MRI and ultrasound can aid in achieving a complete resection of these standard MRI abnormalities. Since we know that gliomas extend beyond the current standard imaging abnormalities,[3,4] the next logical step is to extend the resection beyond these abnormalities. Evidence is starting to accumulate that other modalities like PET and MRSI, or FLAIR MRI in case of enhancing tumors, could guide these extended resections.

A different approach is the use of functional boundaries instead of imaging to guide a resection, whereas intraoperative mapping during awake-surgery defines the limits of resection. This strategy postpones malignant transformation in LGG.[199,200] The pitfall of functional boundaries is the choice of functions to test; removing more of the brain will lead to more deficits depending on how thoroughly the functions are tested. Translating this strategy into accuracy gives a high sensitivity, little residual tumor, but low specificity, not all resected tissue is tumor. A combination of image-guided extended resection and intraoperative stimulation mapping could improve the specificity by removing less normal brain, while keeping a high sensitivity.

FUTURE DIRECTIONS

Randomized clinical trials are needed to compare the influence of image-guided glioma resection based on standard MRI versus the most optimal imaging. In order to determine the most optimal imaging for the detection of glioma infiltration, studies directly comparing different imaging modalities, MRI sequences and combinations of imaging, such as the FRONTIER study,[201] have to be conducted. Besides pre-operative imaging,

intraoperative ultrasound has demonstrated great potential and the results of the randomized US-GLIOMA trial (NCT03531333) are awaited for. Extending the resection implies that more frequently functional areas will be encountered. DCS remains the gold standard for the localization of important brain functions and white-matter tracts. Imaging, however, is indispensable for surgical planning, including the choice of awake versus non-awake surgery. DTI has proven its clinical value in a RCT and studies exploring the increased accuracy of HARDI DTI, possibly in combination with nTMS, are needed.

Niels Verburg
Johannes C. Baayen
Sander Idema
Michiel A.J. Klitsie
Steven Claus
Catharina S. de Jonge
W. Peter Vandertop
Philip C. de Witt Hamer

World Neurosurg 2016 Mar;87:392-8

Chapter 4

In vivo accuracy of a frameless stereotactic drilling technique for diagnostic biopsies and stereoelectroencephalography depth electrodes

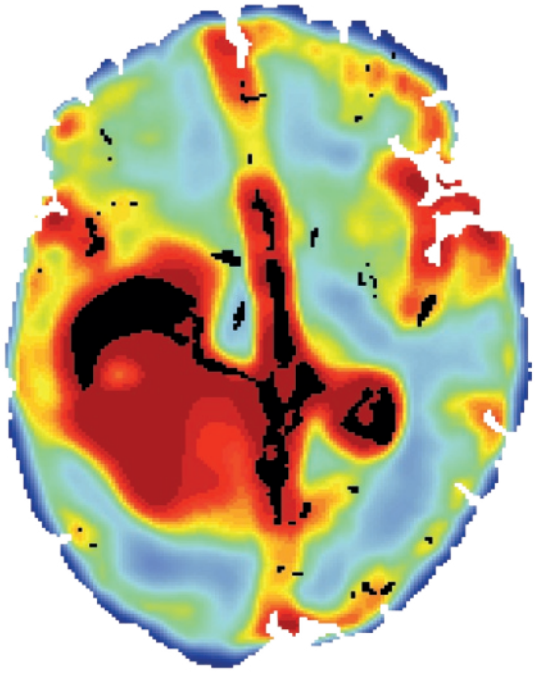

ABSTRACT

Background: Accurate frameless neuronavigation is highly important in cranial neurosurgery. The accuracy demonstrated in phantom models may not be representative for results in patients. Few studies describe the in vivo quantitative accuracy of neuronavigation in patients. The use of a frameless stereotactic drilling technique for stereoelectroencephalography (SEEG) depth electrode implantation in epilepsy patients, as well as diagnostic biopsies, provides a unique opportunity to assess the accuracy with postoperative imaging of preoperatively planned trajectories.

Methods: In seven patients with refractory epilepsy 89 depth electrodes were implanted using a frameless stereotactic drilling technique. Each electrode was planned on a preoperative MR- and CT-scan, and verified on postoperative CT-scan. Following fusion of pre- and postoperative imaging, the accuracy for each electrode was calculated as the Euclidean distance between the planned and observed position of the electrode tip.

Results: The median Euclidean distance between planned and observed electrode implantations was 3.5 mm (95%CI 2.9– .9 mm) with a range of 1.2–13.7 mm.

Conclusion: In this study we showed that the in vivo accuracy of our frameless stereotactic drilling technique, suitable for SEEG depth electrode placement and diagnostic brain biopsies, was 3.5 mm.

INTRODUCTION

Neuronavigation is widely used for diagnostic biopsies, implantation of stereoelectroencephalography (SEEG) depth electrodes and electrodes for deep brain stimulation (DBS), brachytherapy, convection-enhanced delivery and the aspiration of cysts, abscesses and hematomas.[202-207] Frame-based neuronavigation has frequently been replaced by frameless techniques.[208] Advantages of frameless over frame-based techniques are ease of use, more flexible pre-operative planning and less patient discomfort.[86]

The quantitative accuracy of frameless neuronavigation is mostly reported in phantom models.[86] However, these results are not completely representative for clinical accuracy.[209]

Only three studies address the quantitative accuracy of frameless neuronavigation for brain biopsies in patients, with an accuracy varying from 2mm to 4.8mm.[202,210,211] However, multiple publications describe the in vivo accuracy of frameless neuronavigation for implantation of electrodes for DBS, SEEG depth electrodes and Ommaya placement with reported accuracies of respectively 1.7–3.4mm, 2–3.1mm and 4.1mm.[116,203,204,207,212-219]

Recently two studies described a frameless stereotactic drilling technique for implantation of SEEG depth electrodes.[220,221] We use a comparable technique for diagnostic biopsies, as well as SEEG depth electrodes implantation. A comparison of planned and observed depth electrode implantation on postoperative imaging provides the unique opportunity for assessing the quantitative evaluation of the accuracy in clinical practice.

METHODS

Patients

Seven patients, 4 males and 3 females with a median age of 34 years (range, 6–58 years), with medically refractory epilepsy had depth electrode implanted for electroencephalography registration of seizure foci between December 2011 and October 2012 in the VU University Medical Center (VUMC), Amsterdam. All patients underwent extensive preoperative workup including electroencephalography (EEG), computer tomography (CT), magnetic resonance imaging (MRI), positron emission tomography and magnetic encephalography. Indications were therapy resistant epilepsy with discordant neurophysiologic and semiologic findings in all patients.

Approval of the study protocol by the institutional review board (VU University Medical Center, Medical Ethical Research Committee, Amsterdam, The Netherlands) and informed consent were not required according to the Dutch health law of February 26, 1998 (amended March 1, 2006), i.e. Wet Medisch-wetenschappelijk Onderzoek met mensen (WMO; Medical Research Involving Human Subjects Act), Division 1, Section 1.2, because the subjects were not subjected to procedures and were not required to follow rules of behavior outside routine clinical care. Furthermore, the data were analyzed anonymously.

Depth electrode planning

Depth electrode targets were defined by a clinical neurophysiologist of the Epilepsy Institutes of the Netherlands Foundation (SEIN), in conjunction with the department of Neurosurgery of the VU University Medical Center, after evaluating the preoperative workup. Target and entry sites were selected on pre-operative MRI, taking eloquent cortical, subcortical and vascular structures into account. Trajectories were planned using navigation software (iPlan™, BrainLAB AG, Feldkirchen, Germany).

Imaging

Pre-operative imaging included MRI (MAGNETOM Sonata 1.5T or Avanto 1.5T, Siemens; T1-weighted magnetization prepared rapid gradient echo sequence; 1 or 1.5 millimeter (mm) slice thickness; 0.5–1 mm squared pixel size; 265x265 and 512x512 matrix) and navigation CT (SOMATOM Sensation 64, Siemens; 2 mm slice thickness or CT iCT 256, Philips; 1mm slice thickness; 0.4–0.5 mm squared pixel size; 512x512 matrix). The postoperative CT scan, similar to the pre-operative scan protocol, was performed within 4 hours after surgery and fused with the pre-operative CT scan through the navigation software automatic fusion algorithm and manually verified using anatomical landmarks.

Procedure

The complete procedure was executed following a standardized protocol. After general anesthesia the patient was fixed in a head-holder (MAYFIELD, OMI Surgical Products, Cincinnati, USA). Image to patient registration was performed by laser surface matching and manually verified through anatomical landmarks including nasal bridge and tragus. If the surgeon detected registration inaccuracy, the laser registration was repeated or improved by adding extra registration points using a navigated electronic pointer. Subsequently two skin fiducial markers, attached to the patient's forehead and head-holder, were also registered.

The navigated aiming device (VarioGuide™, BrainLAB AG, Feldkirchen, Germany), attached to the head-holder, was adjusted to align the planned trajectory by guidance of the navigation software. The skin, bone and dura were opened using a 3mm drill, stabilized with a guiding channel fixated in the bone. During this procedure the calculated accuracy of the system, as well as the skin fiducials position were monitored for shifts.

After inserting a working channel in the guiding channel the tract for the depth electrode was made using a navigated stylet. A bolt was fixated in the burr hole and the bolt-to-target distance was obtained using the navigation software. Finally the depth electrode with guidewire was inserted in the tract up to the marked distance and, after removing the guidewire, fixated by tightening of the bolt (Figure 1).

For diagnostic biopsies the procedure is similar until the dura is opened. Hereafter a working channel, designed for the biopsy needle, is inserted in the guiding channel and the biopsy is performed following the standard procedure.[222]

Assessment of depth electrode position

Electrode tip position was defined as the last hyperdense signal on the postoperative CT scan. The 3D xyz- DICOM coordinates of the target side and electrode tip were obtained using the navigation planning software (Figure 2).

Statistics

The accuracy was defined as the Euclidean distance between the pre-operative target and electrode tip. This was calculated using the xyz-coordinates and the formula $\sqrt{((x^a - x^b)^2 + (y^a - y^b)^2 + (z^a - z^b)^2}$), where ^{a} is the planned and ^{b} is the postoperative coordinate.

Since the data were not normally distributed accuracy was reported as median distance with 95% confidence intervals (CI). After ranking the measurements from low to high, the ranking position of the measurements was adjusted for the number of measurements per patient. The median was derived from the adjusted 44th and 45th measurement due to the total of 89 measurements. Confidence intervals were assessed using a distribution-free estimation, which requires less assumptions and is more appropriate for smaller data sets.[223] Variation was evaluated by plotting the distance per electrode and calculating the coefficient of variation ((interquartile range/median) x 100) per patient. Finally the median distance with 95%CI per patient was reported.

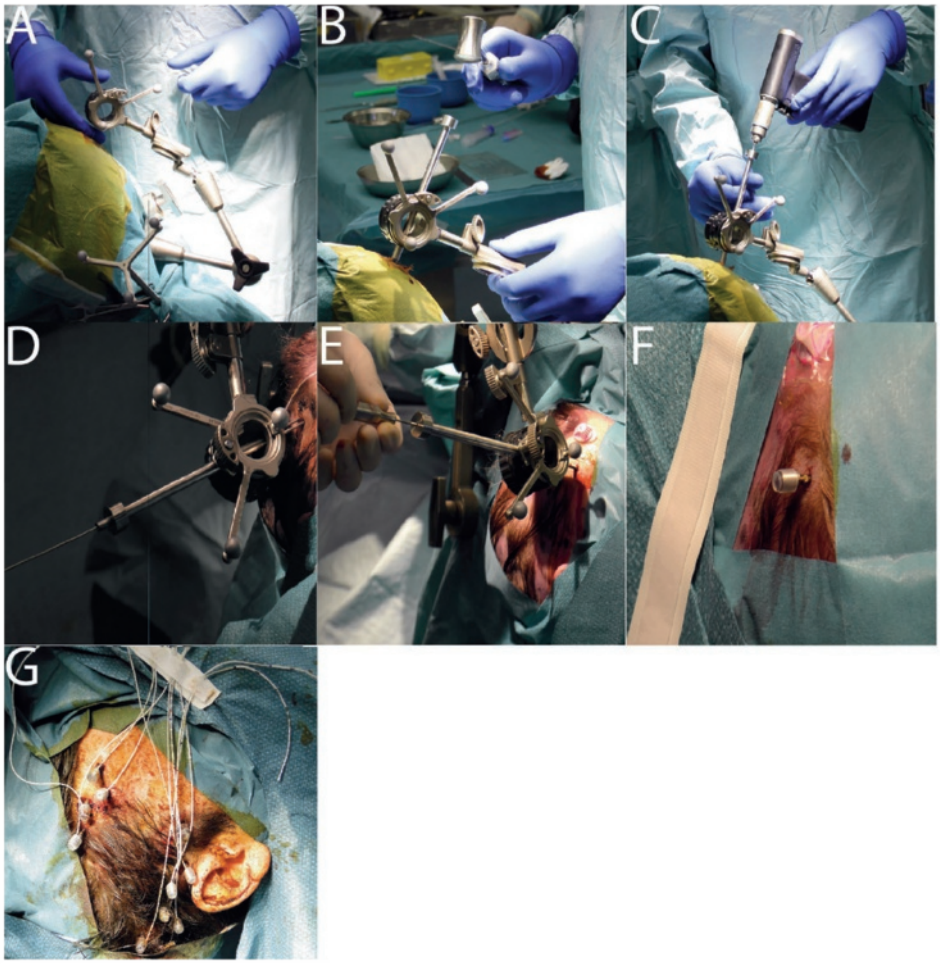

Figure 1 | SEEG depth electrode operation set-up.

A) positioning navigation aiming device. B) fixating guiding channel in the bone of the skull. C) Opening skin, bone and dura with drill. D) Creating tract with stylet through working channel inside guiding channel. E) Fixation of bolt in the burr hole. F) Bolt fixated in the burr hole. G) End of procedure with electrodes placed in tract and fixated in bolt.

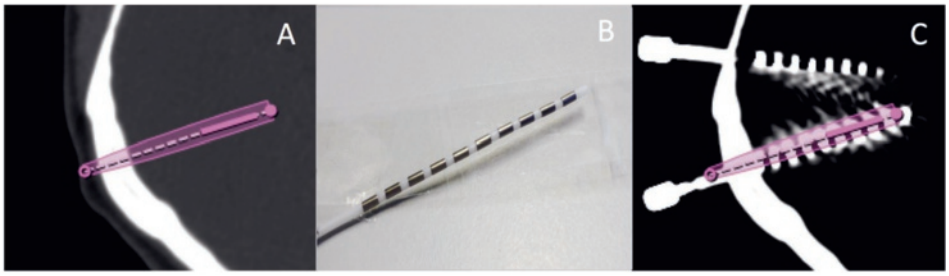

Figure 2 | Illustration of the assessment of a depth electrode position.

A) planned trajectory on pre-operative CT. B) example of depth electrode with the black contact points. C) electrode position on postoperative CT with contact points visible as hyperdense signals and the pre-operative trajectory projected as well.

RESULTS

Eighty-nine depth electrodes were placed (median number of electrodes per patient 12, range 11–15) with temporal (42), frontal (30), occipital (7), insular (5) and parietal (5) localizations of which 56 were left- and 33 right-sided. All onset zones were localized, except for one patient with a temporal regional onset and one patient with focal parietal dysplasia, leading to resective surgery in 3 patients. Two patients were not eligible for surgery; one due to bitemporal onset zones and the other due to worsening of clinical condition due to an intracerebral hemorrhage, after removal of the electrodes, requiring decompressive surgery (Table 1).

The median accuracy was 3.5mm (95%CI 2.9–3.9mm) with a minimum of 1.2 and maximum of 13.7mm (Figure 3). The 13.7mm error occurred in patient 1 due to a temporal located bolt that could only be fixated with extra stiches. Postoperative imaging showed a direct bending of the electrode after entering the cranium.

The coefficient of variation per patient ranged from 28% to 84% (Table 1). The median accuracy per patient ranged from 2.7 to 4.1mm without significant difference between patients (Figure 4).

Table 1 | Patient characteristics.

Patient	Gender	Age	Side*	Location*	DE (n)	Surgery	Accuracy (mm)	CV
1	M	27	R & L	Temporal	15	No	3.7	34%
2	F	6	R	Parietal†	11	No	3.4	84%
3	M	58	L	Temporal‡	12	No	4.1	43%
4	F	34	L	Temporal	15	Yes	3.8	28%
5	F	42	L	Temporal	13	No	2.7	35%
6	M	48	L	Temporal	12	Yes	2.8	55%
7	M	21	R	Frontal	11	Yes	4.0	44%

DE =depth electrodes; CV =coefficient of variation; M =male; F = female; R =right; L =Left * Side and localization of epileptic onset zone. † Onset zone not localized. ‡ Temporal regional onset without distinct onset zone.

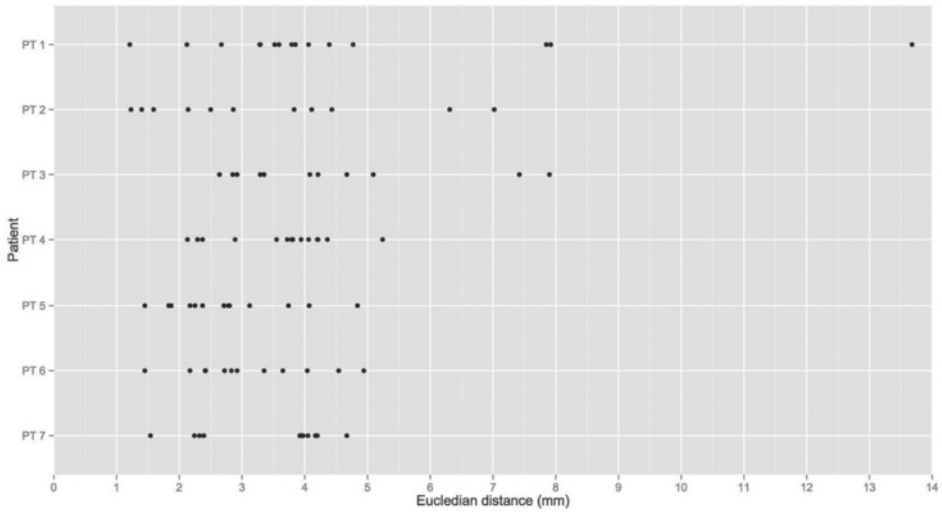

Figure 3 | Euclidean distance of all electrodes plotted per patient.

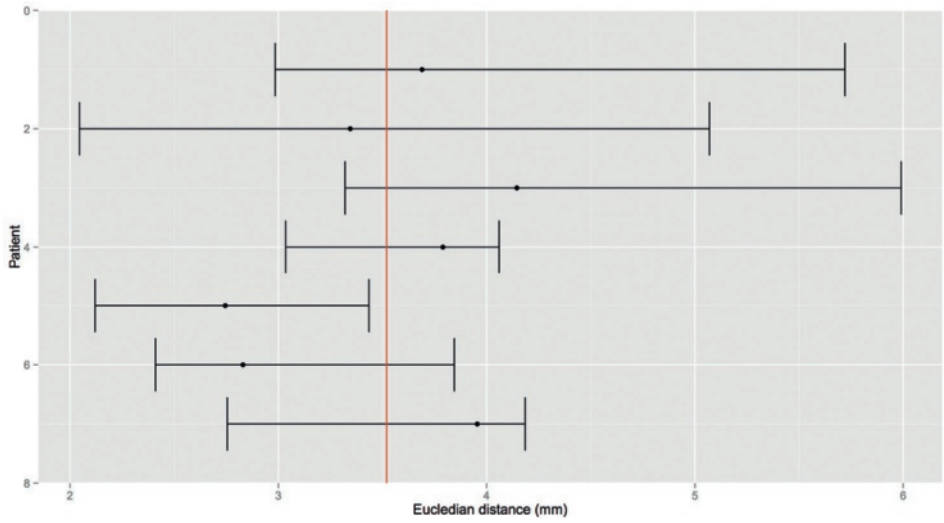

Figure 4 | Median Euclidean distance with 95% confidence intervals per patient with the median Euclidean distance for the group as a red line.

DISCUSSION

In this study we show that our frameless stereotactic drilling technique, used for diagnostic biopsies and SEEG depth electrode placement, has a median accuracy of 3.5mm.

Frameless stereotactic drilling is a modification of the widely used standard stereotactic technique. Recently two different groups published this technique for the first time, with both techniques very comparable to the one used in this study. Dorfer et al. reported a mean Euclidean distance of 3.0mm (maximum 9.4mm) in 26 electrodes.[220] Nowell et al. reported the lateral shift of the electrode compared with planned trajectory, which was 3.6mm (maximum 6.8mm) in 187 electrodes.[221] The mean accuracy of both studies is comparable with this study, although Nowell et al used a different type of error. However the maximum error in both studies is remarkably lower. One outliner in our study, an electrode that diverted directly after entering the cranium, explains this. By excluding this outliner the maximum error is 7.9mm and thus comparable.

In phantom models the mean accuracy of frameless neuronavigation varies between 0.4 and 5.2mm, although the majority is less than 3mm.[209] This is slightly better than the accuracy in this study, which could be explained by patient related variables such as the patient's motion during preoperative screening, inaccuracies in skin fiducial or surface registration, loss of cerebrospinal fluid with possible brain shift or disposition of the head in the head holder.[209]

Four studies describe the quantitative accuracy of frameless neuronavigation for SEEG depth electrodes implantation varying between 2.0 and 3.1mm. Mehta et al. reported 21 patients with 41 electrodes with a mean positioning error of 3.1mm (maximum 7mm) using the frameless StealthStation (Medtronic, Louisville, Colorado, USA).[203] Since the Euclidean distance is the sum of the mean error in three directions it is always larger than the mean positioning error. Taking this into account their results are comparable with ours. Mascott et al. implanted 42 electrodes in seven patients with a mean Euclidean distance of 3.0mm (maximum error 6mm), also using the StealthStation.[224] The major difference with our protocol is the use of skull-based fiducial markers, a variable that was found to improve registration accuracy by the same group.[217] Because of the physical burden for the patient and reasonable minimal improvement of accuracy, we would still advocate surface registration. In the study of Ortler et al. the frameless procedure, using the Treon workstation (Medtronic, Minneapolis, Minnesota, USA), had a mean Euclidian distance of 2.4mm (maximum error 4mm) in 60 electrodes.[218] All of their electrodes were targeted at the hippocampus and placed in the same direction. Our variance in targets and directions and their use of a mouthpiece-based technique could account for difference in mean and maximum accuracy. Finally the robotic system in Cardinale et al. had a median Euclidean distance of 2.0mm (maximum error 15.4mm) in 1567 electrodes.[219] The use of a custom designed robotic arm could explain their superior accuracy, although the maximum error was larger than in the present study. An explanation could be the difference between a surgeon and the robotic feedback system during the operation. Due to the necessary customized setup and high costs this technique is not easily available for other institutions.

Four studies describe the quantitative accuracy of frameless neuronavigation for diagnostic biopsies varying between 2.0 and 4.8mm. Dorward et al. used the EasyGuide Neuro system (Philips Medical Systems Nederland BV, Best, The Netherlands) and measured target localization on postoperative MRI fused with pre-operative data in 15 biopsy sites with a mean Euclidean distance of 4.8mm (maximum 8.1mm).[202] Widmann

et al. used the same method as Dorward et al., except for the Vertek aiming device (Medtronic Inc., Louisville, USA) and postoperative imaging with CT scan. In seven patients air bubbles were found in the trajectory, but only in one patient the target location could be assessed. Therefore they reported trajectory deviation, with a mean error of 4mm and a maximum of 6mm.[210] Willems et al. found a mean Euclidean distance of 3.3mm for bone fiducials and 4.5mm, no maximum reported, for adhesive fiducials using a custom designed microscope based robotic system.[225] The method of the postoperative target assessment in these studies could account for the difference in mean accuracy with the present study. Although to our knowledge there is currently no evidence available, one could imagine that an air bubble or small fluid filled cavity is more prone to brain shift than a catheter. In addition, a study using intraoperative imaging did not find any significant brain shift during and after the placement of depth electrodes.[215] Excluding the outlier in our study, as mentioned above, the maximum error in these studies is comparable with the present study. Bernays et al. assessed navigation accuracy of a stereotactic burr-hole mounted device with intraoperative MRI in 20 patients with a mean Euclidean distance of 2.0mm, however no maximum Euclidian distance was reported.[211] Although the stereotactic technique differs, we believe that the use of intraoperative imaging, allowing for direct correction of errors, explains their superior accuracy. Unfortunately, in the majority of hospitals this facility is unavailable, which makes these results not widely generalizable.

Other methods for analyzing quantitative frameless neuronavigation accuracy are reported. Multiple studies describe the accuracy of deep brain stimulation (DBS) electrode implantation. The majority used skull-based fiducial markers with reported accuracies between 1.7 and 3.4mm.[116,204,212-214] Smith et al. describe the use of an intraoperative O-arm resulting in an accuracy of 3.4mm, while Varma et al. describe a frameless robotic system with an accuracy of 1.7mm.[215,216] The use of skull-based fiducials, intraoperative imaging and robotic systems are commented on above. Lastly, Shamir et al. placed Ommaya catheters with a mean accuracy of 5.9mm.[207] Since their data were not normally distributed it would be appropriate to describe the median, which was 4.1mm. Besides this, our screw fixation technique, compared to the fixation of the Ommaya to the periosteum, could account for less postoperative displacement of the catheters.

Accurate frameless neuronavigation is needed in neurosurgical oncology since diagnostic biopsies are necessary to histologically diagnose critically located or unresectable

gliomas. With new insights in glioma gene expression, leading to improved estimation of prognosis and effectiveness of adjuvant therapy, accurate molecular diagnosis is essential. Due to intratumoral genotypic heterogeneity, [226,227-229] biopsy target selection is becoming of greater importance. Obtaining biopsies from these different targets requires accurate neuronavigation techniques such as presented in this study.

The strengths of this study are the large number of measurements; robust assessment of accuracy by postoperative electrode position; reporting Euclidean distance and the use of this technique for both SEEG depth electrode placement and diagnostic biopsies. A limitation of our study is the possible 'pullout' effect after electrode placement resulting in an increased error, although this effect is reduced due to our screw fixation technique. The use of anatomical based registration instead of skull-based fiducials could have influenced our registration accuracy as well, but as mentioned above it does not justify the invasiveness of the skull-based technique. Since postoperative air can cause brain shift, this could have influenced the accuracy.[215,230] Lastly, image fusion of the pre- and postoperative CT does introduce an error, which has to be taken into account.

CONCLUSION

In this study we showed that the in vivo accuracy of our frameless stereotactic drilling technique, suitable for SEEG depth electrode placement and diagnostic brain biopsies, was 3.5mm. This is comparable with other frameless techniques described in the literature.

Niels Verburg
Petra J. W. Pouwels
Ronald Boellaard
Frederik Barkhof
Otto S. Hoekstra
Jaap C. Reijneveld
W. Peter Vandertop
Pieter Wesseling
Philip C. De Witt Hamer

Neurosurgery 2016 Oct;79(4):535-40

Chapter 5

Accurate delineation of glioma infiltration by advanced PET/MR neuro-imaging (FRONTIER study): a diagnostic study protocol

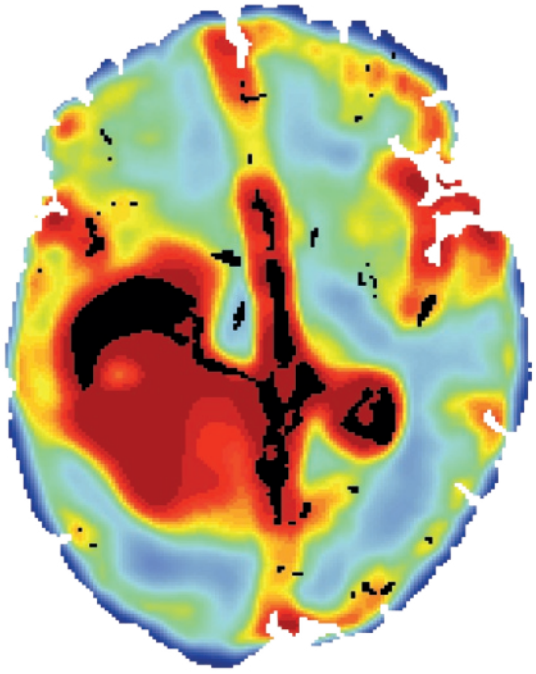

ABSTRACT

Background: Glioma imaging, used for diagnostics, treatment planning and follow-up, is currently based on standard magnetic resonance imaging (MRI) modalities (T1 contrast-enhancement for gadolinium-enhancing gliomas and T2/ Fluid attenuated inversion recovery (FLAIR) hyperintensity for non-enhancing gliomas). The diagnostic accuracy of these techniques for the delineation of gliomas is suboptimal.

Objective: To assess the diagnostic accuracy of advanced neuroimaging compared with standard MRI modalities for the detection of diffuse glioma infiltration within the brain.

Methods: A monocenter, prospective, diagnostic observational study in adult patients with a newly diagnosed, diffuse infiltrative glioma undergoing resective glioma surgery. Forty patients will be recruited in three years. Advanced neuroimaging will be added to the standard preoperative MRI. Serial neuronavigated biopsies in and around the glioma boundaries, obtained immediately preceding resective surgery, will provide histopathological and molecular characteristics of the regions of interest, enabling comparison with quantitative measurements in the imaging modalities at the same biopsy sites.

Expected outcome: We hypothesize that a combination of positron emission tomography, MR spectroscopy and standard MRI will have a superior accuracy for glioma delineation compared to standard MRI alone. In addition, we anticipate that advanced imaging will correlate with the histopathological and molecular characteristics of glioma.

Discussion: In this clinical study, we determine the diagnostic accuracy of advanced imaging in addition to standard MRI to delineate glioma. The results of our study can be valuable for the development of an improved standard imaging protocol for glioma treatment.

RATIONALE AND BACKGROUND INFORMATION

Gliomas represent 80–90% of parenchymal brain tumors in adults with an incidence of 5.9 per 100.000 person-years: approximately 1000 patients per year in The Netherlands.[158] Most gliomas show extensive infiltration in the brain parenchyma. These so-called diffuse gliomas universally recur, without exception resulting in death despite standard treatment, which consists of as extensive as possible resection, followed by radiation and chemotherapy.

Both resective surgery and adjuvant radiation therapy are based on T1 contrast-enhancement for gadolinium-enhancing gliomas and on T2/ Fluid attenuated inversion recovery (FLAIR) hyperintensity volume outlines for non-enhancing gliomas. This strategy is founded on early and preliminary observations, and has remained unchanged since.[3,70] Diffuse gliomas recur locally in the vast majority of patients, even after seemingly radical surgical removal and radiation therapy with 2cm margins. This, and the fact that glioma infiltration has been demonstrated to extend up to two centimeters beyond standard MRI outlines, underscores that up till now delineation of these neoplasms has been less than optimal.[4,5,231,232]

Several publications provide arguments for underestimation of the spread of diffuse gliomas using standard MRI and potential benefit from advanced MRI and positron emission tomography (PET) imaging. Advanced imaging, such as diffusion-weighted imaging (DWI), perfusion-weighted imaging (PWI), magnetic resonance spectroscopy (MRS) and PET, has been shown to be able to identify tumor in areas of normal standard MRI signal.[53,129,233]

Our study addresses a clinically relevant research question, which so far has not been adequately answered: What is the best neuroimaging approach to discriminate areas with glioma infiltration from brain tissue without glioma cells?

STUDY GOALS AND OBJECTIVES

The goal of this study is thus to determine the best neuroimaging approach for glioma delineation.

The specific objectives are:

- To assess the increase in diagnostic accuracy of adding advanced neuroimaging modalities to standard MRI for the detection of diffuse glioma infiltration within the brain.
- To correlate the information obtained by standard and advanced imaging to histologic and molecular characteristics of the tissue.

We hypothesize that advanced neuroimaging, in combination with standard MRI, will have a superior diagnostic accuracy in comparison with standard MRI alone. Besides, we hypothesize that histological and molecular characteristics of (different areas of) glioma will correlate better with advanced imaging than with standard imaging.

STUDY DESIGN

The study design is a monocenter, prospective, diagnostic observational study.

METHODOLOGY

Subjects

Inclusion criteria. Patients of 18 years and older with a MRI interpretation of a diffuse glioma by an experienced neuroradiologist, and who have an indication for resective surgery; the indication confirmed by the multidisciplinary neuro-oncology tumor board.

Exclusion criteria. Patients who are pregnant or have undergone previous brain surgery, cranial irradiation or chemotherapy. Patients with other brain pathology on MRI, such as stroke or multiple sclerosis. Patients with a tumor located infratentorially or in the spinal cord.

Withdrawal criteria. Patients who do not successfully undergo one PET scan. A summary of all criteria is given in Table 1.

Table 1 | Inclusion/Exclusion/Withdrawal criteria.

Inclusion criteria	Exclusion criteria	Withdrawal criteria
Adult (18 years and older)	Previous brain surgery, cranial radiotherapy or chemotherapy	Not successfully undergoing one PET scan
MRI interpretation of diffuse glioma by an experienced neuroradiologist	Other brain pathology on MRI, such as infarction or multiple sclerosis	
Indication for resective surgery confirmed by the multidisciplinary neuro-oncology workgroup	Tumor located infratentorially or in the spinal cord	
	Pregnancy	

STUDY DESCRIPTION

The study is separated into two phases (Figure 1). In both phases, standard and advanced imaging will be performed pre-operatively (Table 2). Immediately preceding resective surgery, serial image-guided neuronavigated biopsies in and around the glioma boundaries will be obtained using a stereotactic drilling technique.[234] Two samples are collected from each biopsy location, one for assessment of histopathological characteristics and one for molecular analysis.

Phase I is designed to decide on the optimal PET tracer, to simplify PET scanning methodology and to develop a robust MRI protocol for glioma volume estimation. Eight patients will receive a dynamic PET protocol with invasive blood sampling, and image-derived carotid input function for metabolite analysis of

[^{18}F-]Fluoroethyl-tyrosine (FET) and [^{11}C-]Choline (CHO) tracers, as well as advanced MR imaging. The data obtained will be used to establish a simplified PET protocol and to determine which of both PET tracers will be further pursued in the next study phase.

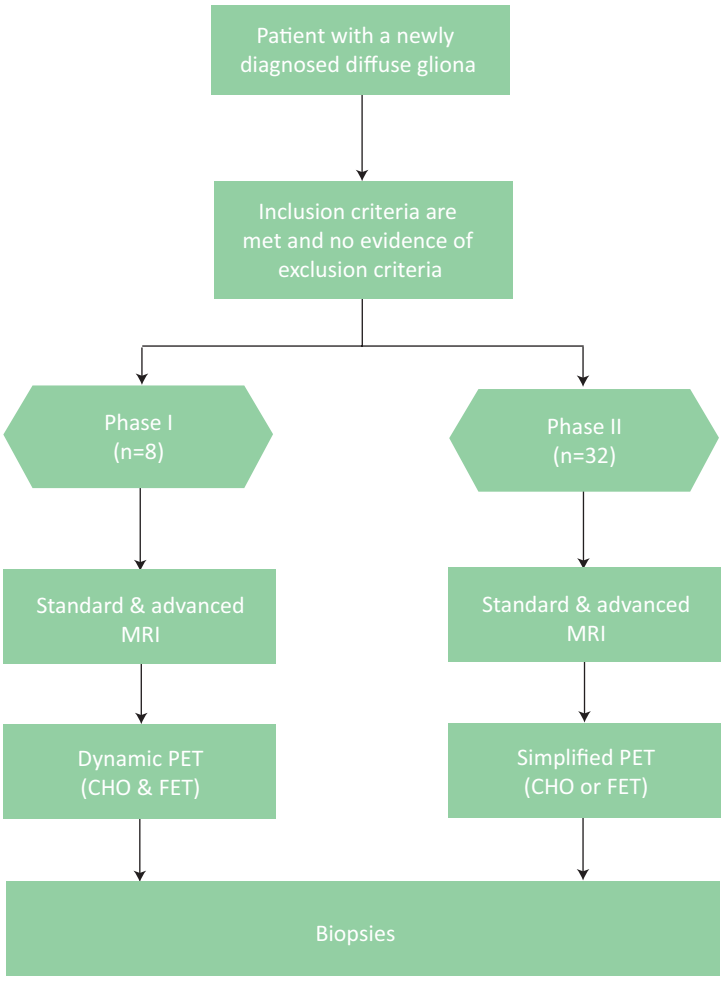

Figure 1 | Imaging protocol for different phases study.

Cho =^{11}C-Choline, FET =[^{18}F]Fluoroethyl-tyrosine

To obtain a total sample size of 20 patients with a high-grade glioma (WHO grade III or IV) and 20 with a low-grade glioma (WHO grade II), 20 additional patients will receive single advanced MRI and selected simplified PET imaging in the second phase to complete the data acquisition according to the sample size calculation for the main research question.

Table 2 | Quantitative imaging parameters.

Modality/Technique	Parameter 1	Parameter 2	Parameter 3
Standard MRI			
2D T1	T/N ratio		
2D T2	T/N ratio		
3D FLAIR	T/N ratio		
2D T1 after contrast	T/N ratio		
3D T1 after contrast	T/N ratio		
Advanced MRI			
3D MRS	T/N ratio	Cho/NAA ratio	
ASL	T/N ratio	relative CBF	
DTI	T/N ratio	FA	ADC
DSC	T/N ratio	relative CBV	relative CBF
PET			
^{11}C-Choline	T/N ratio	SUV	Net influx rate
[^{18}F]Fluoroethyl-tyrosine	T/N ratio	SUV	Net influx rate

OUTCOME MEASURES

MRI

MRI will be performed using the Philips Achieva whole-body 3.0T MR-scanner, equipped with the standard head coil. Table 2 shows the different techniques.

PET

PET will be performed using the Philips Gemini time-of-flight (TOF) PET-CT scanner or the Philips Ingenuity TOF PET/MRI-scanner. After intravenous administration of 370 Megabecquerel (MBq) of [^{15}O]H_2O a 10 min dynamic scan is acquired. This is followed by a 40min dynamic scan after injection of 200 MBq CHO. With a minimum of 4 hours after injection of CHO the FET scan will be performed the same day using 200MBq FET and a scan time of 90 minutes. During the scans manual blood samples are withdrawn in order to calibrate the online collected arterial input functions and to derive a fully metabolite-corrected plasma input function.

Of each biopsy site qualitative (high, normal or low signal) and quantitative parameters will be acquired by an experienced neuroradiologist and a nuclear medicine physician (Table 2).

Pathology

Of each biopsy location one sample will be processed for histopathological analysis and the other sample for molecular analysis. Histopathological analysis will be performed using hematoxylin-and-eosin (H&E) staining and immunohistochemical markers to assess cellularity, glioma infiltration, proliferation, microvascular changes, and necrosis. Molecular analysis will include assessment of DNA mutations, deletions, amplifications and RNA expression profiling. Two experienced neuropathologists will evaluate independently, and blinded for the imaging results, all biopsies and designate those as: normal brain tissue; diffuse glioma with few, moderate or many tumor cells in a background of pre-existent brain tissue; highly cellular glioma without (apparent) preexistent brain tissue remaining; uninformative.

DISCUSSION

Few studies investigate the diagnostic accuracy of glioma delineation, and most of these studies assess only one or two imaging modalities. This can at least partly be explained by the logistic challenge of multimodality preoperative imaging and of obtaining multiple image-guided biopsies. Nevertheless, studies that provide a direct comparison of multiple imaging modalities with histopathological data are necessary to determine the optimal imaging modality for the delineation of diffuse gliomas. Using combined PET-MRI will help to reduce the number of scans necessary for multimodality imaging, while frameless stereotactic techniques will facilitate the acquisition of multiple image-guided biopsies with good accuracy within a limited time.

The importance of adequate glioma delineation is underscored by reports describing that (near) radiologically complete resection of MRI abnormalities (T1-weighted gadolinium-enhanced MRI for HGG and on T2/FLAIR-weighted MRI for LGG) is correlated with improved survival.[8,235-239] A resection based on modalities with superior delineation could result in even more complete resection and thus holds promise for even longer survival, and conversely to identify patients with glioma infiltration beyond meaningful surgical therapy, so that useless, and possibly harmful, resections can be avoided. Moreover,

evidence accumulates that subsequent therapeutic modalities are more successful after resection that is as complete as possible. [238]

TRIAL STATUS

Patient recruitment was initiated on September 1, 2014.

SAFETY CONSIDERATIONS

Because neuronavigated biopsy has a risk of less than 2% of intracranial hemorrhage with consequences for the patient, the number of biopsy trajectories is limited to three.[240,241] Since the biopsy procedure is immediately followed by a craniotomy for tumor resection, possible hemorrhages can be directly identified and removed. The tumor resection will be performed according to standard care.

All adverse events reported spontaneously by the subject or observed by the investigator or his staff will be recorded in the protocol case report forms (CRF) using the Common Terminology Criteria for Adverse Events classification.[242] All serious adverse events (SAEs) will be reported through the web portal ToetsingOnline (https://www.toetsingonline.nl) to the accredited Medical Ethical Committee (METC) that approved the protocol. SAEs that result in death or are life threatening are reported expeditiously.

FOLLOW-UP

All patients will receive standard follow-up, which consists of postoperative clinical admission for as long as needed and an outpatient appointment eight weeks after the procedure. Apart from that, postoperative adjuvant chemo- and/or radiotherapy will be installed according to histopathological and molecular classification of the tumor, as discussed postoperatively at the neuro-oncology tumor board meetings. All adverse events will be followed until they have abated, or until a stable situation has been reached.

DATA MANAGEMENT AND STATISTICAL ANALYSIS

Data will be collected on electronic CRF (eCRF). The eCRF is only assessable by the principal and the study investigator. The eCRF will be completed on site by an investigator. The principal investigator will review the collected data.

The number of biopsies and patients required to compare the area under the curve (AUC) of the receiver operating characteristic (ROC) curves depend on the reference AUC (t1), the minimal relevant AUC from the improved imaging (t2), the ratio of non-tumor and tumor biopsies (ratio), the correlation of imaging within patients (r), the average number of biopsies per patient (s), the correlation of histopathological quantification between biopsies within patients (rho), the type I error (alpha) and the type II error (beta).[243-245] Under the assumptions of t1 0.6, t2 0.8, ratio 0.25, r 0.5, s 6, rho 0.2, alpha 0.05 and beta 0.2, 20 patients per glioma target volume subgroup are required. The overall study population then comprises 20 non-enhancing and 20 enhancing glioma patients, each stratum providing at least 120 biopsies. For testing the correlation between simplified and full quantitative measurement of input function in dynamic PET scanning a sample size of eight is mostly used in pilot studies. Due to the experience with other trials we will include this number in phase I. In phase II 32 patients will be included to obtain the total of 40 patients from our sample size calculation.

Continuous variables will be described as a mean with standard deviation if the distribution is symmetric and as a median with minimum and maximum if it is skewed. Categorical variables are presented as numbers with percentages. Data analysis will be performed using R. AUCs are compared using a nonparametric resampling test using pROC in R.[246-248] Next, multivariate logistic regression analysis modeling histopathology by quantitative imaging is performed using Bayesian models.

QUALITY ASSURANCE

As the METC of VU University Medical Center (VUmc) decided it was unnecessary to appoint a Data Safety Monitoring Board for this study, the progress of this study will be monitored by the Clinical Research Bureau of VUmc.

EXPECTED OUTCOMES OF THE STUDY

We expect that advanced imaging in combination with standard imaging, will have a superior diagnostic accuracy for glioma delineation compared with current standard imaging. This delineation could help neurosurgeons, neurologists, radiation oncologists and medical oncologists in their clinical decision-making. Next, studies comparing glioma resection or radiotherapy using standard versus standard plus advanced imaging can be conducted to investigate possible influences on clinical outcome.

The expected correlation between advanced imaging and histologic and molecular characteristics could provide biomarkers for prognosis and choice of therapy, as well as further insight into glioma imaging

DURATION OF THE PROJECT

We anticipate that phase I will take 12 months and phase II 24 months, aiming for a total study duration of three years.

PROJECT MANAGEMENT

The principal investigator, Dr. de Witt Hamer, will lead the study. Dr. Pouwels will be responsible for the MRS data, Dr. Barkhof for the MRI data, Dr Boellaard and Dr. Hoekstra for the PET data, and Dr. Wesseling for the pathology data. The study investigator, Mr. Verburg, MSc, will coordinate the logistics and of the study as well as the interpretation of the results.

ETHICS

The study is approved by the METC of VUmc and will be conducted according to the principles of the Declaration of Helsinki and in accordance with the Medical Research Involving Human Subjects Act. Explicit written consent will be obtained from all patients in this study.